

Article

Optimization and Demonstration of Direct LD Pumped High-Power Fiber Lasers to Balance SRS and TMI Effects

Lingfa Zeng¹, Xiaolin Wang^{1,2,3,*}, Li Wang¹, Yun Ye¹, Peng Wang^{1,2,3}, Baolai Yang^{1,2,3}, Xiaoming Xi^{1,2,3}, Zhiyong Pan^{1,2,3}, Hanwei Zhang^{1,2,3}, Chen Shi^{1,2,3}, Kai Han^{1,2,3} and Xiaojun Xu^{1,2,3}

¹ College of Advanced Interdisciplinary Studies, National University of Defense Technology, Changsha 410073, China

² Nanhu Laser Laboratory, National University of Defense Technology, Changsha 410073, China

³ Hunan Provincial Key Laboratory of High Energy Laser Technology, National University of Defense Technology, Changsha 410073, China

* Correspondence: chinaphotonics@163.com

Abstract: Up to now, transverse mode instability (TMI) and stimulated Raman scattering (SRS) have become the main factors limiting the power scaling of conventional ytterbium-doped fiber laser. Many technologies are proposed to suppress the SRS or TMI individually, but most of them are contradictions in practical application. In this article, we focus on the technologies that can balance the suppression of both SRS and TMI, including fiber coiling optimization, pump wavelength optimization, pump configuration optimization, and novel vary core diameter active fiber. Firstly, we validate the effectiveness of these technologies in both theoretical and relatively low-power experiments, and introduce the abnormal TMI threshold increasing in a few-mode fiber amplifier with fiber coiling. Then, we scale up the power through various types of fiber lasers, including wide linewidth and narrow linewidth fiber lasers, as well as quasi-continuous wave (QCW) fiber lasers. As a result, we achieve 5–8 kW fiber laser oscillators, 10–20 kW wide linewidth fiber laser amplifiers, 4 kW narrow linewidth fiber amplifiers, and 10 kW peak power QCW fiber oscillators. The demonstration of these new technical schemes is of great significance for the development of high-power fiber lasers.



Citation: Zeng, L.; Wang, X.; Wang, L.; Ye, Y.; Wang, P.; Yang, B.; Xi, X.; Pan, Z.; Zhang, H.; Shi, C.; et al. Optimization and Demonstration of Direct LD Pumped High-Power Fiber Lasers to Balance SRS and TMI Effects. *Photonics* **2023**, *10*, 539.

<https://doi.org/10.3390/photronics10050539>

Received: 27 March 2023

Revised: 18 April 2023

Accepted: 25 April 2023

Published: 6 May 2023



Copyright: © 2023 by the authors. Licensee MDPI, Basel, Switzerland. This article is an open access article distributed under the terms and conditions of the Creative Commons Attribution (CC BY) license (<https://creativecommons.org/licenses/by/4.0/>).

Keywords: high-power fiber laser; ytterbium-doped fiber; transverse mode instability; stimulated Raman scattering; pump wavelength; pump configuration; fiber coiling

1. Introduction

High-power ytterbium-doped fiber laser is an ideal light source for industrial processing, such as laser cutting and laser welding. In the past 20 years, the output power of fiber laser has achieved a leap from hundreds of watts to 10 kW level [1–16]. According to the current public reports, the technology of fiber lasers with output power exceeding 10 kW has gradually matured, and the difficulty lies in achieving high power and high beam quality (that is, high brightness) simultaneously. Brightness is a physical quantity related to the power and beam quality of laser, which is defined as follows [17,18]:

$$B = \frac{P}{(M^2\lambda)^2} \quad (1)$$

where, P , λ , and M^2 represent the power (W), wavelength (μm), and beam quality of the laser, respectively. When applied to quasi-continuous wave (QCW) fiber lasers, P should be the peak power of the laser. Under the same output power, the smaller the value of the beam quality, the higher the brightness of the laser. From the characteristics of the laser, under the same power, after focusing by the same system, the light spot at the focus of the high-brightness laser is smaller and the energy density is higher. High-brightness fiber laser

is very important to improve the processing speed and product quality in new industries. Therefore, the development of fiber lasers in the future must consider the simultaneous improvement of power and brightness.

From the current development situation, fiber lasers based on single fiber are still an effective way to achieve high-beam quality lasers. However, due to the nonlinear effect especially stimulated Raman scattering (SRS) and transverse mode instability (TMI), the difficulty of realizing high power and high beam quality laser based on a single fiber increases rapidly [19,20]. At present, many technologies are proposed to suppress the SRS or TMI individually. However, under normal circumstances, their restraining measures are contradictory in practical application. For example, to suppress SRS, it is necessary to increase the core diameter, enhance the pump absorption and shorten the length of the fiber, while the suppression of TMI needs to reduce the core diameter, weaken the pump absorption, and increase the length of the fiber. How to balance SRS and TMI has become a key issue. Among them, TMI has received extensive research in recent years.

TMI was discovered in 2010 [21–26]. At present, the thermal effect in fiber is considered the physical origin of TMI, and the sources of heat mainly include quantum defect, photon darkening, and background loss [27–30]. Since 2010, a lot of research has been carried out on the suppression of TMI in fiber lasers, which can be divided into passive suppression and active suppression in general. Considering the mode control in the fiber, the optimization of the fiber structure is carried out to suppress the higher-order modes, which is conducive to improving the TMI threshold. These special fiber designs include photonic band gap fiber, large pitch fiber (LPF), confine doped fiber, multi-core fiber, and so on [31–48]. In addition, fiber coiling is also an effective measure to improve the TMI threshold by suppressing higher-order modes [6,49–51]. Starting from the physical origin of TMI, we can design anti-photon darkening fiber to suppress TMI [52]. Relevant research mainly focuses on the optimization of fiber doping composition, doping concentration, and fiber materials. For these measures, there is still much work to be done before they are put into practical application. We can also optimize the signal and pump wavelengths to alleviate the quantum defect [53–64]. In addition, the pump absorption of the fiber can be optimized to reduce the temperature gradient in the fiber, inhibit the formation of long-period refractive index gratings, and suppress TMI. In addition to the above passive measures, there are also active measures to suppress TMI, such as signal and pump modulation [65–68]. However, passive measures will not increase the complexity of the system and will have more potential.

Fiber lasers are mainly divided into tandem pump and direct laser diode (LD) pump. Among them, the tandem pump configuration has obvious advantages in suppressing TMI, but the efficiency is relatively low; the system is complex and the cost is high [69–71]. Therefore, more and more researchers focused on the direct LD pumped technology to realize high-power fiber lasers. In LD pumped fiber lasers, there are few technologies such as counter-pump configuration which can suppress the SRS and TMI simultaneously. In this article, we focus on the suppression techniques for achieving balance between SRS and TMI without deteriorating either of them, including fiber coiling optimization, pump wavelengths optimization, pump configuration optimization and novel vary core active fiber.

At present, the influence of pump wavelength on TMI reported by other groups is mostly theoretical analysis, lacking systematic experimental research [53,55,58,60,63]. In terms of fiber coiling, TMI is restrained by reducing the fiber coiling diameter [51]. In recent years, with the goal of achieving a high-power fiber laser with high beam quality, we have been focusing on balancing SRS and TMI by optimizing the pump wavelengths and pump configuration. In the aspect of fiber coiling, we found the abnormal phenomenon of increasing the TMI threshold by increasing the fiber coiling diameter [10,72]. In addition, we propose varying core diameter active fiber represented by tapered fiber, spindle-shaped fiber, and saddle-shaped fiber, which can balance SRS and TMI in the fiber and break through the power limit of conventional fiber [73–81].

In this work, we will focus on the optimization and demonstration of the technologies that balance the suppression of both SRS and TMI, including common methods such as fiber coiling, pump configurations, and novel methods including pump wavelength optimization and various core active fiber. We first verify the effectiveness of these technologies at relatively low power and introduce the abnormal TMI threshold increasing in a few-mode fiber amplifier with fiber coiling optimization. Additionally, then we scale up the power in fiber laser oscillators, fiber laser amplifiers both in wide linewidth and narrow linewidth, as well as quasi-continuous wave (QCW) fiber lasers. With these technologies, we have achieved laser power from 4 kW to 20 kW in fiber laser oscillators and fiber laser amplifiers.

2. Theoretical and Simulation Study of the Measures for Suppressing SRS and TMI

In this section, we will theoretically demonstrate the suppression of TMI and SRS in fiber lasers by pump configuration optimization, pump wavelength optimization, fiber coiling optimization, and varying novel core fiber. These measures can balance the suppression of both SRS and TMI or, at least, do not deteriorate them.

2.1. Nonlinear Effect (SRS) and TMI Suppression Based on Pump Optimization

Pump optimization, especially the counter-pump configuration, is one of the measures that can mitigate both the SRS and TMI. Here, we will first study the nonlinear effect and the TMI suppression based on pump optimization. B-integral is often used in high-power fiber laser systems to evaluate the nonlinear effects of the system. The definition of B-integral is shown in Equation (2) [82,83]. Where n_2 represents the nonlinear refractive index of the fiber, and its value is completely determined by the fiber itself. The calculation of B-integral in fiber lasers is relatively complex. However, as shown in Equation (2), its value is directly proportional to the power integral along the longitudinal direction of the fiber. Therefore, the power integral can be used to approximate the B-integral in the laser, thereby evaluating the nonlinear effects. The simulation in this section is mainly divided into two steps. First, calculate the power distribution in the fiber according to the rate equations of the fiber laser, and then use the power distribution to calculate the power integration along the longitudinal direction ($\int P(z)dz$). The obtained value can be used to evaluate the nonlinear effect on the laser.

$$B = \frac{2\pi}{\lambda} \int n_2 |E(r, t)|^2 dz \propto \int P(z) dz \quad (2)$$

The simulated laser adopts a fiber laser amplifier based on MOPA (master oscillation power amplification) structure. The parameters of the fiber and the main parameters used in the simulation are shown in Table 1. The simulation results are shown in Figure 1. Figure 1a shows the power distribution in the fiber under different pump configurations. From the evolutionary trend, the laser power in the fiber increases rapidly at the front end of the fiber under the co-pump configuration, while it is mainly concentrated at the end of the fiber under the counter-pump configuration. Figure 1b shows the normalized B-integral calculated according to Equation (2) based on the data in Figure 1a. It is obvious that under the three pump configurations, the value of B-integral is the largest under the co-pump configuration. The values are about 68% and 36% for the bidirectional pump and counter-pump configurations, respectively. This fully shows that for three pump configurations, the counter-pump configuration has the most obvious advantage in suppressing SRS, followed by the bidirectional pump configuration, and the co-pump configuration has the strongest SRS. It is worth noting that due to the lack of consideration for fiber coiling and the loss of the fiber itself, the calculation results show that the output power of the laser is highest in the co-pump configuration, followed by bidirectional pump configuration, and then the lowest in the counter-pump configuration. However, considering losses and coiling, the impact on power will only be a few watts and will not affect the entire power distribution curve. Therefore, the impact on integration is not significant and does not affect the comparison under different pump configurations.

Table 1. Main parameters for simulation of fiber laser amplifier.

Parameters	Value
Core/Cladding diameter	25/400 μm
Signal wavelength	1080 nm
Seed power	100 W
Pump wavelength	976 nm
Length of active fiber	12 m
Cladding pump absorption coefficient	1.68 dB/m
Pump configuration (power)	co-pump (1000 W) Counter pump (1000 W) Bidirectional pump (500 W of co-pump and 500 W of Counter pump)

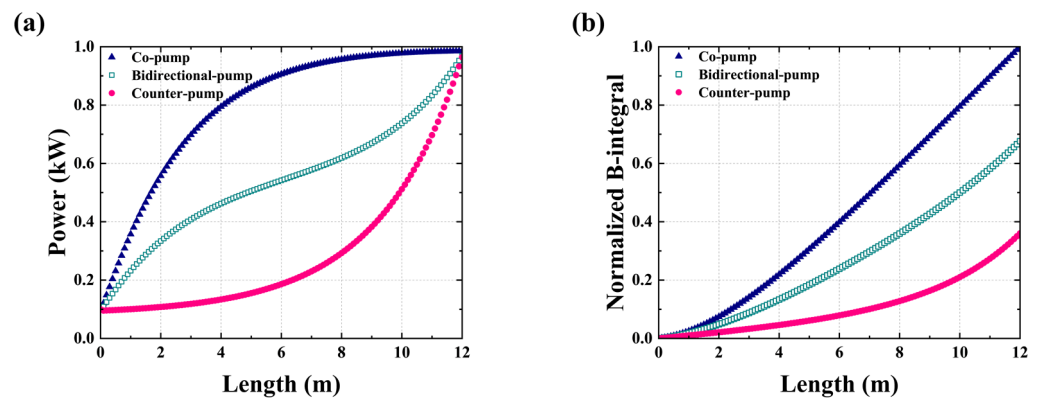


Figure 1. Power distribution and normalized B-integral in fiber amplifier under different pump configurations. (a) The power distribution in the amplifier. (b) Normalized B-integral.

According to the semi-analytic theoretical model of TMI in the fiber amplifier, we can calculate the TMI threshold under different pump configurations. The detailed theoretical model and derivation process can be seen in Ref. [57]. In this model, TMI is judged by the high order mode ratio (HOM ratio), and the derived expression of the HOM ratio (ζ) is shown in Equation (3). The physical means of each parameter in Equation (3) are shown in Table 2. Referring to the conclusion in Ref. [84], we set the signal power when ζ reaches 5% as the TMI threshold of the laser.

$$\begin{aligned} \zeta(L) &= \zeta_0 \exp \left[\int_0^L dz \iint g(r, \phi, z) (\Psi_2 \Psi_2 - \Psi_1 \Psi_1) r dr d\phi \right] \\ &+ \frac{\zeta_0}{4} \sqrt{\frac{2\pi}{\int_0^L P_1(z) |\chi''(\Omega_0, z)| dz}} \\ &\times \exp \left[\int_0^L dz \iint g(r, \phi, z) (\Psi_2 \Psi_2 - \Psi_1 \Psi_1) r dr d\phi \right] R_N(\Omega_0) \exp \left[\int_0^L P_1(z) \chi(\Omega_0, z) dz \right] \end{aligned} \quad (3)$$

Table 2. The parameters in Equation (3) and their physical means.

Parameter	Physical Meaning	Parameter	Physical Meaning
ζ_0	Initial high-order mode components	g	Gain distribution in lasers
Ψ_1	Normalized mode field distribution of LP01 mode	Ψ_2	Normalized mode field distribution of LP11 mode
P_1	Power distribution of LP01 mode	χ''	Second derivative of χ with respect to Ω
R_N	Relative intensity noise of input signal	χ	Nonlinear coupling coefficient between LP01 and LP11
L	The length of active fibers	Ω	Frequency shift between LP01 and LP11
Ω_0	Maximum coupling frequency shift	r, ϕ	Transverse distribution of active fiber

Here, the fiber parameters in our simulation are consistent with those in Table 1, with a pump wavelength of 976 nm. The results are shown in Figure 2. In a co-pump configuration, the TMI threshold of the laser is 774 W. In contrast, the TMI threshold under the counter-pump configuration is 1067 W, which is 37.9% higher than that in co-pump configuration. This is due to the stronger gain saturation effect in the counter-pump configuration. The results in Figures 1 and 2 comprehensively demonstrate the advantages of counter-pump configuration in suppressing SRS and TMI. It should be noted that our purpose here is only to compare the TMI thresholds under the co-pump and counter-pump configurations. The actual fiber coiling is not considered in the simulation, so the TMI threshold of the laser will be lower than the actual results. Therefore, in actual lasers, the proportion of counter-pump power can be increased to effectively suppress SRS and TMI.

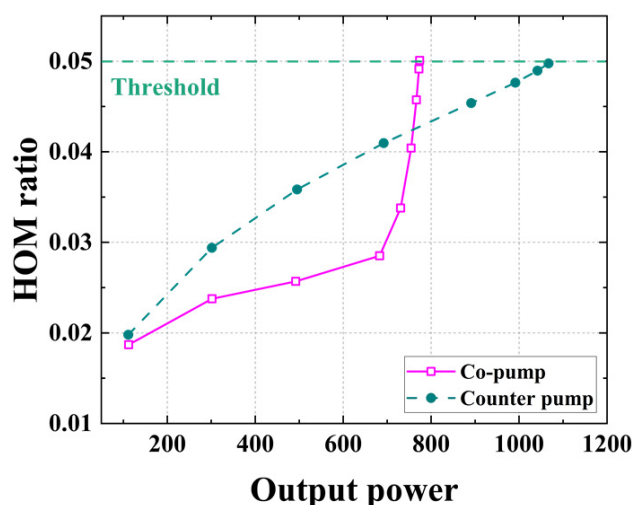


Figure 2. Simulation of TMI thresholds in co-pump configuration and counter-pump configuration.

2.2. TMI Suppression Based on Pump Wavelength Optimization

The simulation in Section 2.1 shows the impact of pump configurations on SRS and TMI. In contrast, the influence of pump wavelength on TMI is greater. Here, we will theoretically introduce the effect of pump wavelength on TMI. The core/cladding diameter of the active fiber used in the simulation is 30/400 μm , and the doping concentration of Yb^{3+} is $6.3 \times 10^{25} \text{ m}^{-3}$. In order to ensure sufficient pump absorption when the pump wavelength is changed, the fiber length is selected as 20 m. Considering the absorption cross-sections and quantum defects of ytterbium-doped fibers at various wavelengths, we chose to calculate wavelengths of 915 nm, 969 nm, 976 nm, 981 nm, and 982 nm, respectively. The simulation results can also be compared with our previous experiments [61,85]. The simulation results are shown in Figure 3b and Table 3. The simulation results show that the TMI threshold of the laser is the highest when the pump wavelength is 985 nm, followed by 982 nm, 981 nm, 969 nm, 915 nm, and 976 nm. The optimization of pump wavelength needs to consider two factors, one is the absorption cross-section of Yb^{3+} (as shown in Figure 3a), and the other is the quantum defect between the pump wavelength and signal wavelength. In a comprehensive consideration, optimizing the pump wavelength in the long wave direction can not only reduce the absorption coefficient but also reduce the quantum defect, which is more beneficial to the suppression of TMI. Therefore, when the pump wavelength is 981 nm, 982 nm, or 985 nm, the calculated TMI threshold is relatively high. Near the absorption peak of Yb^{3+} , the absorption cross-section changes rapidly with the wavelength, and the wavelength change has a great impact on TMI. For example, although there is only 1 nm difference between 982 nm and 981 nm, the threshold value has increased by 15.2%. When the wavelength offset is large, the absorption cross section will be small. In order to ensure sufficient pump absorption, the length of fiber needs to be increased, which is not conducive to SRS suppression. Therefore, the wavelength shift of the pump

should not be too large, and the range of 981 nm to 985 nm in the calculation is a relatively suitable range for balancing SRS and TMI. It is worth noting that in this section, we used ytterbium-doped fibers that are different from those in Section 2.1, but this does not affect the respective conclusions.

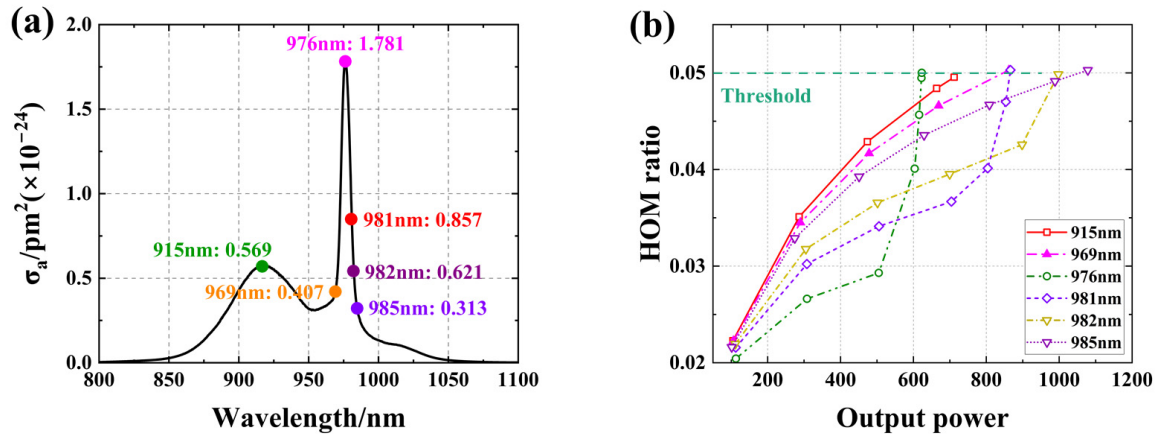


Figure 3. (a) Absorption cross section of Ytterbium-doped fiber and (b) Simulation results of TMI threshold at different pump wavelengths.

Table 3. The pump power when TMI appears at different pump wavelengths.

Wavelength	915 nm	969 nm	976 nm	981 nm	982 nm	985 nm
TMI threshold (Signal)	711 W	862 W	623 W	866 W	998 W	1079 W
Quantum efficiency	84.7%	89.7%	90.4%	90.8%	90.9%	91.2%
Absorption cross section	5.6932×10^{-25}	4.0733×10^{-25}	1.7669×10^{-24}	8.5664×10^{-25}	6.2079×10^{-25}	3.1281×10^{-25}

2.3. TMI Suppression Based on Fiber Coiling

Different from the above two schemes, the effect of fiber coiling on TMI is somewhat complex. When the fiber is coiled, each mode will result in some loss. In general, the loss of higher-order mode (HOM) is greater than that of the fundamental mode (FM), so TMI can be suppressed by coiling the fiber and increasing the loss of HOM [6]. At present, many reports have verified the feasibility of suppressing TMI by optimizing fiber coiling theoretically and experimentally. Here, we also calculate the TMI threshold of fiber lasers with different coiling radii based on the semi-analytic theoretical model of TMI in fiber lasers. The simulation is based on the fiber amplifier structure. The power of LP01 mode and LP11 mode in the initial injected signal is 20 W and 0.2 W, respectively, which can be considered as a single-mode input. The core/cladding diameter of the active fiber is 20/400 μm , and the pump wavelength is 976 nm. In our theoretical model, when the fiber coiling length is long, the accumulation of HOM loss is large, and the calculated TMI threshold is very high. Therefore, we set the total length of the coiling fiber to be 1 m, and the variation of the TMI threshold with the coiling diameter is also credible. The simulation results are shown in Figure 4. With the decrease of the coiling radius, the TMI threshold of the laser gradually increases and becomes more and more sensitive to the fiber coiling. It shows that with the decrease of coiling diameter, the filtering effect of HOM becomes increasingly effective, and the content of HOM is lower at the same power level. The simulation results show that the TMI threshold of the laser can be increased by reducing the coiling diameter of the fiber under the condition of single-mode injection.

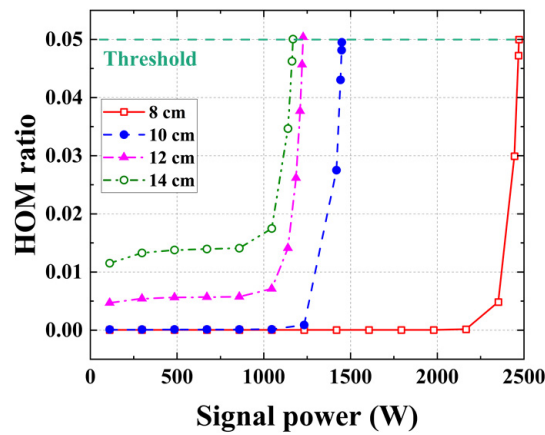


Figure 4. Simulation results of TMI threshold under different coiling radii.

Figure 4 shows the normal TMI phenomenon where the TMI threshold increases with the decrease of fiber coiling diameter. In addition, introducing a mode loss after fiber coiling will also lead to mode field distortion, resulting in coupling between modes. A combination of various factors may also lead to an abnormal TMI phenomenon where the TMI threshold increases with the increase of the fiber coiling diameter. So, we also simulated the mode excitation and TMI threshold under different higher-order mode power ratios when the single-mode laser is injected into fibers with different coiling diameters based on the theory of mode field distortion and mode coupling [86,87]. The results are shown in Figure 5. As shown in Figure 5a, when the coiling diameter increases from 20 cm to 30 cm, the proportion of the FM in the output laser increases gradually. At the same time, it also means a decrease in the HOM ratio. A decrease in the HOM ratio may lead to an increase in the TMI threshold. Figure 5b shows the TMI thresholds calculated under different HOM ratios (η) in injected lasers. Based on Figure 5a,b, it can be inferred that the decrease in η caused by the increase in fiber coiling diameter may lead to an increase in the TMI threshold. In this experiment, we have observed the abnormal TMI phenomenon related to fiber coiling diameter, which will be described in Section 3.3.

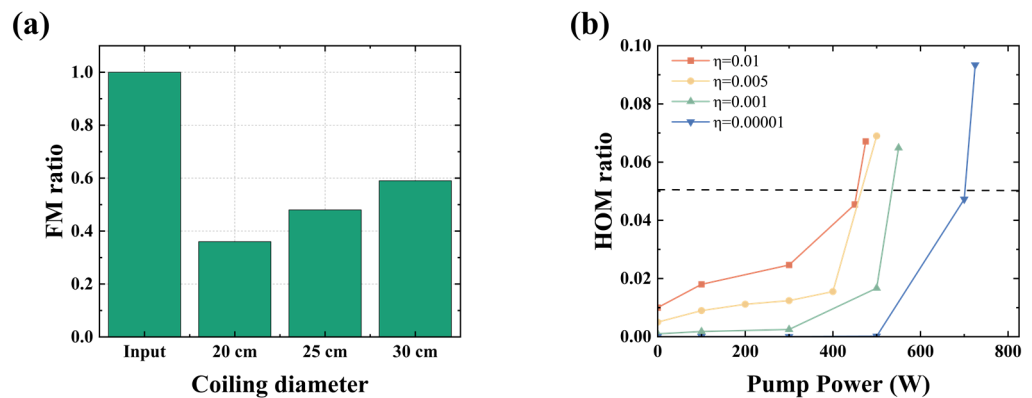


Figure 5. Simulation results of mode excitation and TMI threshold during fiber coiling. (a) The ratio of the FM in the input and output laser varies with the coiling diameter; (b) TMI threshold at different HOM ratios (η) in the inject laser.

2.4. Balance TMI and SRS Based on Vary Core Diameter Active Fiber

Compared with pump configuration optimization, pump wavelength optimization, and fiber coiling optimization, the new structure fiber is a more potential implementation scheme for high-power fiber lasers. Among them, vary core diameter active fiber (VCAF), represented by spindle-shaped fiber (SPF), has received more and more attention in recent years. In order to theoretically demonstrate the balance of VCAF on SRS and TMI in fiber lasers, we simulated SRS and TMI in fiber amplifiers based on spindle-shaped fiber and

uniform fiber, respectively. The main parameters of the simulated fibers are shown in Table 4. Wherein, Fiber1 is an SPF with a constant core-to-cladding ratio. Fiber2, Fiber3, and Fiber4 are uniform fibers with constant core and cladding diameters. The doping and core-to-cladding ratio of the four fibers are consistent, and the same pump absorption can be guaranteed under the condition of the same fiber length. In addition, according to the definition of equivalent core diameter in Ref. [78], the equivalent core diameter and an equivalent cladding diameter of Fiber1 are 25 μm and 500 μm , respectively. Therefore, the results of the data comparison between Fiber1 and Fiber3 are also convincing.

Table 4. Main parameters of fibers used in simulation.

Fiber	Core Diameter (Distribution)	Cladding Diameter (Distribution)	Length
Fiber1	20–30–20 μm	400–600–600 μm	16 m
Fiber2	20 μm	400 μm	16 m
Fiber3	25 μm	500 μm	16 m
Fiber4	30 μm	600 μm	16 m

The simulation results are shown in Figure 6. Among these fibers, the calculated TMI thresholds are in the order of Fiber2, Fiber1, Fiber3, and Fiber4 from high to low. The SRS intensity at the output end of the active fiber is from weak to strong in the order of Fiber4, Fiber3, Fiber1, and Fiber2. The order of the two is completely opposite, that is, the higher the TMI threshold, the higher the possibility of the corresponding laser being limited by SRS, and vice versa. The role of the application of spindle fiber is to balance SRS and TMI. From the results, Fiber1 can reach the TMI threshold close to that of Fiber2 and has an SRS suppression capability similar to that of Fiber3 and Fiber4. After proper parameter optimization, SPF can achieve a balance between SRS and TMI, and achieve higher output power. In addition to SPF, VCAF such as tapered fiber (TF) and saddle-shaped fiber (SAF) also have the same ability.

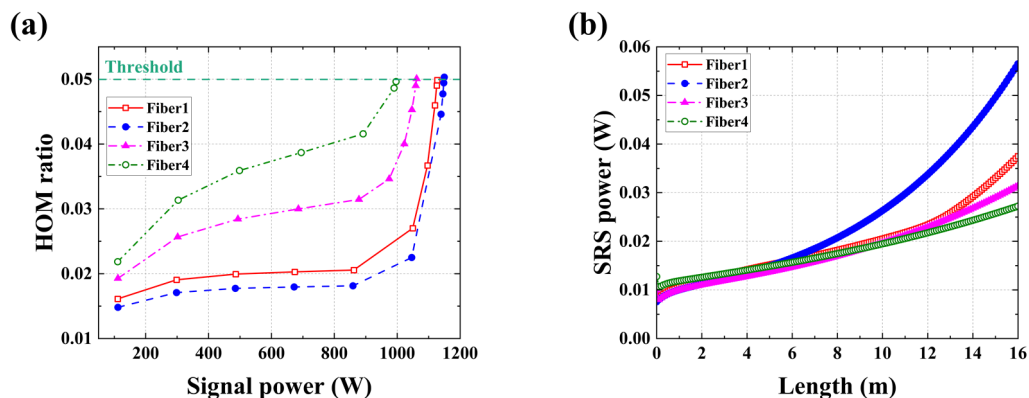


Figure 6. Simulation results of TMI and SRS in SPF and uniform fiber. (a) The HOM ratio in different fibers varies with the output signal power; (b) SRS power at different locations in different fibers.

2.5. Summary

The simulation of the above sections, respectively, verified the advantages of pump configuration optimization for SRS and TMI suppression, the advantages of pump wavelength and fiber coiling optimization for TMI suppression, and the good balance of VCAF for SRS and TMI. Specifically, the counter-pump configuration can weaken the nonlinear effect and suppress TMI. The optimization of the pump wavelength can make the heat distribution in the laser more uniform which means a higher TMI threshold [29,61,85,88]. For fiber coiling, on the one hand, it will increase the loss of HOMs; on the other hand, it will also lead to the coupling between modes, so its effect on TMI needs to be discussed

separately. VCAF is a new type of fiber with great potential, and there have been many experimental reports. In general, the above inhibition measures have been verified in the experiment. In the following content, we will describe the verification of the above schemes in the experiment and introduce its application in high-power fiber lasers.

3. Experimental Demonstration of These Measures on SRS and TMI Suppression in Direct LD Pumped Fiber Laser

3.1. SRS in Lasers under Different Pump Configurations

According to the simulation results in Section 2.1, SRS in the laser is the weakest in the counter-pump configuration. Based on the structure of the oscillating-amplifying integrated fiber laser, we compared the SRS of the laser under the co-pump and the counter-pump configurations. The structure of the laser is shown in Figure 7. The active fiber in the oscillating section is commercial fiber with a core/cladding diameter of 22/400 μm and the active fiber in the amplifying section is 25/400 μm fiber with low absorption. Combined with LDs with a central wavelength of 981 nm as the pump source, the laser has a high TMI threshold, which is conducive to comparing SRS under different pumping configurations. The results are shown in Figure 8. In the co-pump configuration, when the output power is 2170 W, the SRS intensity in the output laser is only 14 dB lower than the signal. In the counter-pump configuration, no obvious SRS is observed when the output power is 2584 W. When the output power reaches 4359 W, the SRS intensity is still 21 dB lower than the signal. Under this experimental condition, if the consistent SRS intensity is controlled, the output power that can be achieved in the counter-pump configuration is more than twice that in the co-pump configuration. The results of the experiment well illustrate the inhibition effect of counter-pump configuration on SRS. In the bidirectional pump configuration, the higher the proportion of counter-pump power, the better the SRS suppression effect. Therefore, in the laser system that is not limited by TMI, the counter-pump configuration can maximize the output power of the laser.

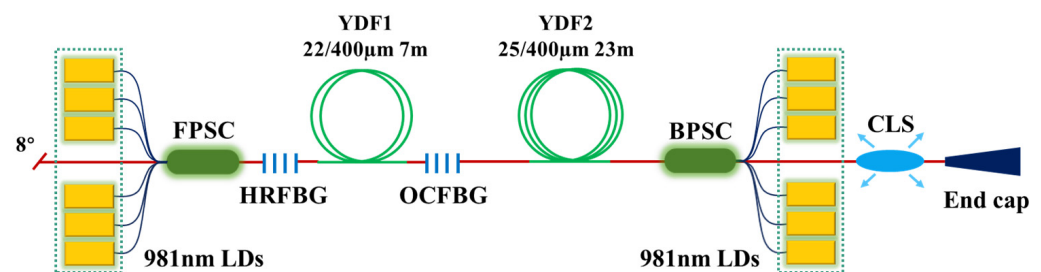


Figure 7. Schematic diagram of oscillating-amplifying integrated fiber laser.

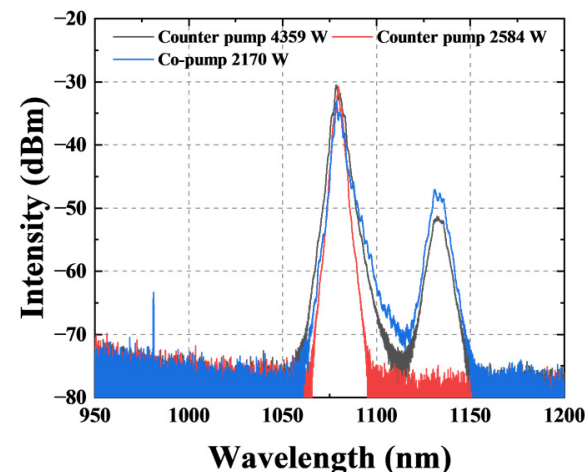


Figure 8. Output spectrum of laser under different pump configurations.

3.2. TMI Suppression by Optimizing Pump Wavelength

As mentioned in the introduction, the measures to suppress TMI by optimizing the pump wavelength can be traced back to 2014 [54,55]. However, most of the early studies remained at the theoretical stage, lacking systematic experimental verification. We have systematically designed and customized wavelength-stabilized (WS) LDs with central wavelengths of 969 nm (WS-969) and 981 nm (WS-981), respectively. It is applied to the high-power fiber laser, and the TMI threshold of the laser is compared with that of the lasers pumped by common LDs, including wavelength stabilized LDs with a central wavelength of 976 nm (WS-976), LDs with central wavelengths of 915 nm (915). In the past few years, we have designed an experimental platform with a low TMI threshold to verify the suppression ability of pump wavelength optimization to the TMI [61,62,85,88]. The TMI threshold of the laser pumped by WS-981 and WS-969 is 2.2 times and 3.45 times that of the laser pumped by WS-976 under the same conditions [61,85].

In addition, the TMI with different pump wavelengths at high power has also been studied. The laser is a fiber amplifier based on the MOPA structure, as shown in Figure 9. The active fiber of the amplifier adopts double-cladding YDF with a core/cladding diameter of 25/400 μm, and its total length is 30 m. The absorption coefficient of the active fiber for pump light with a wavelength of 915 nm is 0.56 dB/m, the core NA is 0.06, and the minimum coiling diameter is 85 mm. In the process of pump wavelength optimization, only the pump modules of the laser are optimized, while the rest remain unchanged.

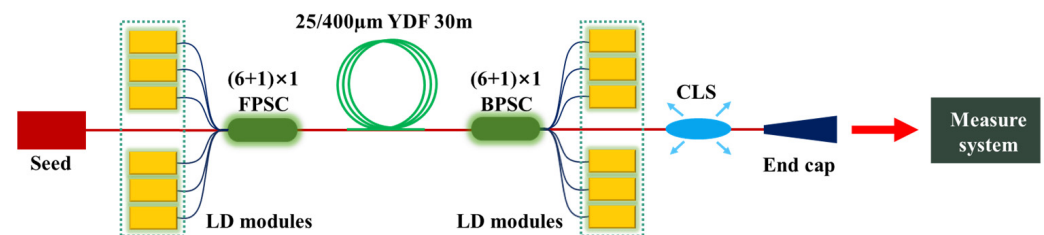


Figure 9. Schematic diagram of the fiber amplifier based on pump wavelength optimization.

The experimental results are shown in Figure 10. Figure 10a shows the variation of output power and efficiency with pump power when applying WS-981, 915, and WS-976 for bidirectional pumps and the variation of output power and efficiency with pump power when applying WS-969 for counter-pump. For LDs with different wavelengths, lasers can maintain good efficiency. When applying WS-969, due to the lower total pump absorption, the efficiency of the laser is slightly lower than that when applying other LDs. In the experiment, when applying WS-976 and 915, and WS-981 as pump sources, the performance of the laser was tested under co-pump, counter-pump, and bidirectional pump, respectively. When applying WS-969, only tests were conducted under the counter-pump configuration. Figure 10b shows the maximum output power obtained from all experiments and lists the corresponding limiting factors. The maximum power with WS-976 is 3027 W, which is limited by TMI. When applying WS-981 and 915, the maximum output power reached 5030 W and 4489 W, respectively, both limited by SRS. Limited by the total available pump power, when applying WS-969, only experiments with a counter-pump configuration were conducted, and the maximum output power reached 4073 W, which is the maximum output power under the condition of a unidirectional pump with different LDs. The laser has the highest TMI threshold (greater than 4073 W under the counter-pump configuration) when unidirectional pumped by WS-969. These results show that suppressing TMI through pump optimization is an effective way to improve the output power of fiber lasers.

3.3. Abnormal TMI Suppression Method Based on Fiber Coiling

The appearance of TMI is often accompanied by the degradation of beam quality, indicating that higher-order modes play an important role in the emergence of TMI. From

this point of view, the way to suppress TMI through fiber design and fiber coiling is proposed. The optimization of fiber coiling is an effective way. The normal view is that the TMI threshold of the laser increases with the decrease of the coiling diameter, which has been verified theoretically and experimentally. However, we found the abnormal TMI suppression method that the TMI threshold increases with the increase of coiling diameter. In [72], we realized the fiber laser amplifier with 30/400 μm fiber, and found that when the minimum coiling diameter of the fiber gradually increased from 9 cm to 12 cm, the TMI threshold of the laser gradually increased. Subsequently, we design a high-power fiber laser amplifier based on the double-cladding YDF with a core/cladding diameter of 30/600 μm. The YDF of the amplifier is coiled in a cylindrical fiber groove. The TMI threshold of the laser with a fiber coiling diameter of 13–16 cm is measured under the condition of WS-976 and WS-981 pumped. The structure of the laser is shown in Figure 11. The laser adopts a counter-pump configuration, as described in Sections 2.1 and 3.1, which can best suppress SRS.

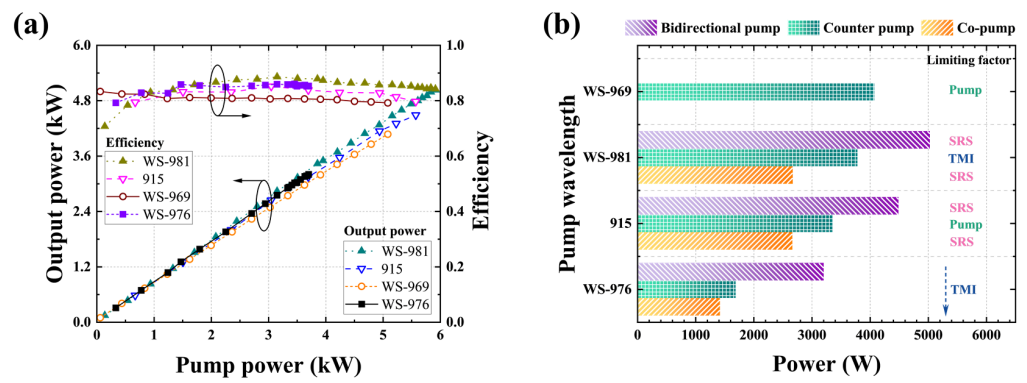


Figure 10. Main experimental results of fiber amplifier based on pump wavelength optimization. (a) The variation of output power and efficiency with pump power when applying WS-981, 915, and WS-976 for a bidirectional pump, and the variation of output power and efficiency with pump power when applying WS-969 for counter-pump. (b) The maximum output power and corresponding limiting factors under LDs with different wavelengths and pump configurations.

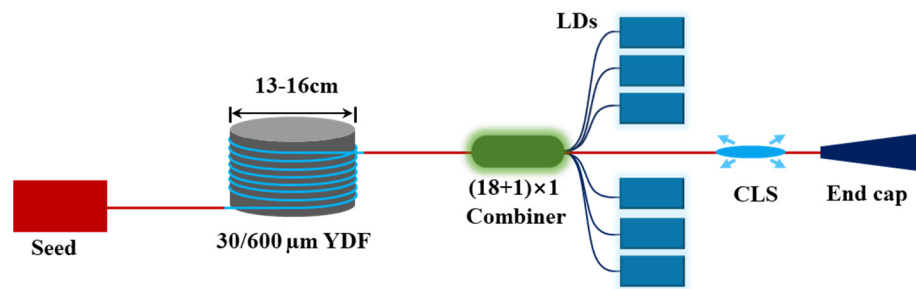


Figure 11. The structure diagram of 30/600 μm fiber laser amplifier with optimized fiber coiling.

The results are shown in Table 5. With the increase of fiber coiling diameter, the TMI threshold of the laser increases gradually. When the coiling diameter is more than 13 cm, the TMI threshold of the laser is more than twice that of the WS-976 pump when the WS-981 is used as the pump source. As mentioned in the simulation in Section 2.3, the smaller the coiling diameter of the few-mode fiber (the current fiber core diameter is 30 μm, which can support multiple modes), more higher-order modes will be excited during the laser amplification process and will not be filtered, thus reducing the TMI threshold. In addition, the brightness of the output laser is calculated according to Equation (1). Under the same fiber coiling diameter, optimizing the pump wavelength can improve the output power and brightness of the laser. At the same pump wavelength, although the beam quality of the output laser may be slightly degraded (affected by fiber fusion), the improvement of

the maximum output power also brings the improvement of the brightness of the laser. In fact, similar abnormal TMI phenomena were reported as early as 2019, and in recent years, there have been reports of increasing the TMI threshold by introducing higher order modes [89–91]. In [90], they believe that introducing higher-order modes without frequency shift from the fundamental mode (which will not affect TMI) can reduce the pump gain of higher-order modes with frequency shift from the fundamental mode (which will affect TMI), thereby increasing the TMI threshold.

Table 5. The result of the TMI threshold after optimizing the fiber coiling diameter.

Pump Wavelength	Coiling Diameter	M ² of Seed after Pass the Amplifier	M ² at Maximum Output Power	TMI Threshold	Brightness	Ratio
976 nm	13 cm	1.58	2.24	1516 W	259.0	1.00
	14 cm	1.73	2.23	1680 W	289.6	1.11
	15 cm	1.75	2.10	3130 W	608.5	2.06
	16 cm	1.85	2.04	4321 W	890.2	2.85
981 nm	13 cm	1.58	2.24	2788 W	476.4	1.84
	14 cm	1.73	1.86	3975 W	985.1	2.62
	15 cm	1.79	2.06	6960 W	1406.1	4.59
	16 cm	1.87	2.17	>7100 W	1292.7	>4.68

3.4. Balance TMI and SRS in Fiber Laser Amplifier Based on VCAF

Theoretical research has proved that VCAF can balance SRS and TMI in high-power fiber lasers. We successively designed two experiments to compare TMI and SRS in spindle-shaped fiber (SPF) and uniform fiber [76,92]. The lasers in the experiment are all fiber laser amplifiers based on the MOPA structure. The fiber parameters for comparison are shown in Table 6. The two kinds of fibers used in the respective control experiments are from the same fiber preform, which can ensure the consistency of fiber parameters. In the TMI comparison, the uniform fiber used has the same equivalent core diameter as the SPF. WS-976, with a lower TMI threshold, is used as the pump source to eliminate the impact of SRS. In the contrast experiment of SRS, WS-981 was used as the pump source to eliminate the influence of TMI. This part of the research has been reported in detail in [76,92], and is only briefly introduced here.

Table 6. Parameters of fibers used for SRS and TMI comparative experiment in fiber laser amplifier.

Experimental Objectives	Experimental Parameters	Fiber Parameters
TMI comparison	WS-976 pump	Uniform fiber, 28/600 μm, core NA: 0.065, absorption coefficient: ~0.80 dB/m@976 nm
		Spindle-shaped fiber, constant cladding diameter, (CCTC fiber in Figure 12) 20–36–20/600 μm, core NA: 0.065, absorption coefficient: ~0.78 dB/m@976 nm
SRS comparison	WS-981 pump	Uniform fiber, 25/400 μm, core NA: 0.060, absorption coefficient: ~0.81 dB/m@976 nm
		Spindle-shaped fiber, constant core-to-cladding ratio, 25/400–37.5/600–25/400 μm, core NA: 0.060, absorption coefficient: 0.78 dB/m@976 nm

The results are shown in Figure 12. In the amplifier based on the SPF, under the co-pump and counter-pump configurations, obvious fluctuations appear in the time domain signal of the laser when the power reached 1324 W and 2494 W, respectively, which shows that the TMI threshold of the laser is 1324 W and 2494 W, respectively under different pump

configurations. For the amplifier based on uniform fiber, the TMI threshold measured under the same conditions was 1135 W and 2056 W, respectively. The results show that VCAF represented by SPF has better TMI suppression capability than uniform fiber. Figure 12c shows the experimental results of SRS in SPF and uniform fiber (SSR represents the SRS suppression ratio). When using SPF and uniform fiber, the laser can achieve a 6 kW laser output with similar beam quality under the condition of a bidirectional pump. However, from the SRS point of view, there is obvious SRS when a uniform fiber is used. When SPF is used, there is no obvious SRS, indicating that SPF has better SRS inhibition ability. Based on the above two experiments, VCAF has the advantage of balancing SRS and TMI in the fiber laser. Additionally, the parameters of fiber have optimization potential, which can be designed according to the actual situation.

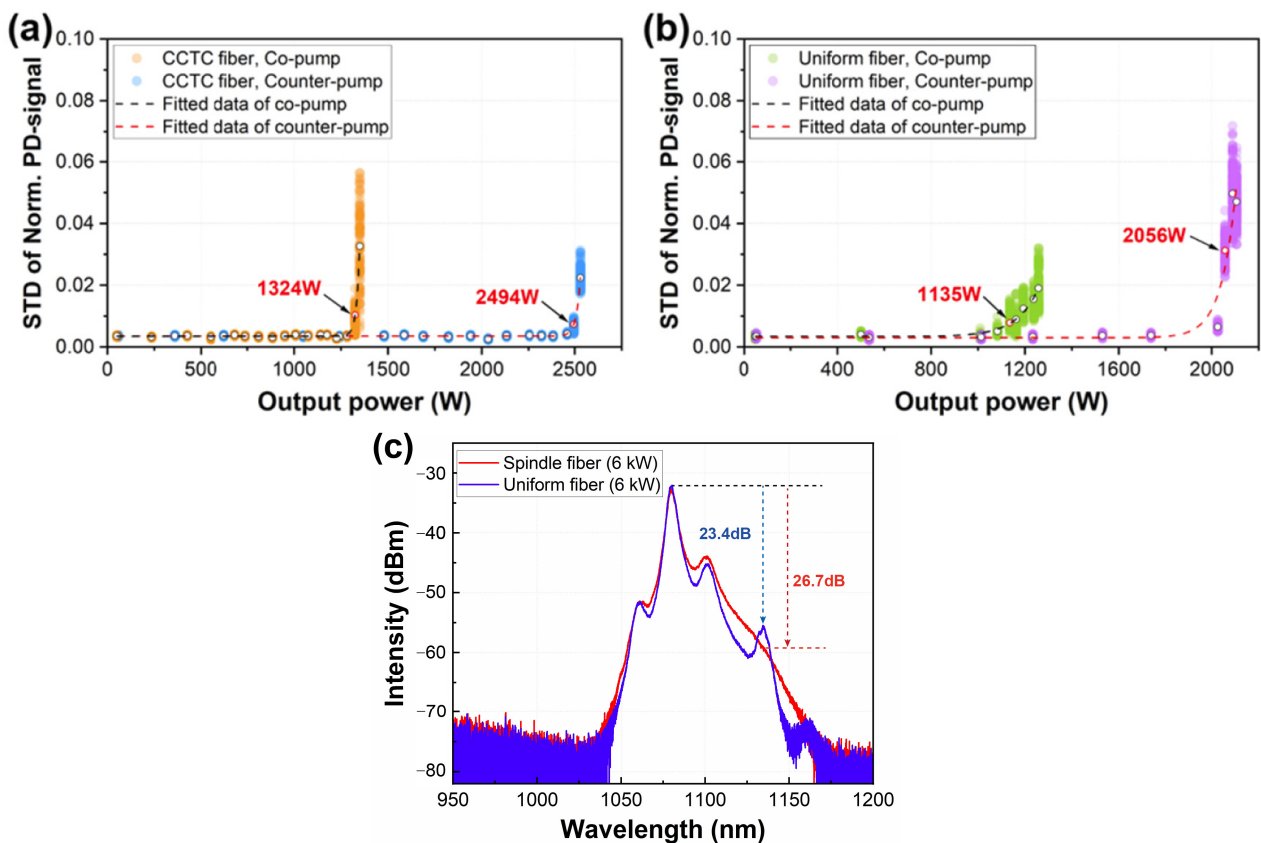


Figure 12. The results of the TMI and SRS comparative experiment in the fiber amplifier based on SPF and uniform fiber. (a,b) STD curve of PD signal when compared to TMI. (c) Output spectrum when compared to SRS [76,92].

3.5. Summary

In this section, we introduce the experimental verification of several new technical schemes mentioned in Section 2 in turn. From the respective results, the role of the new technical solution for SRS and TMI in fiber lasers is obvious. It is noteworthy that we introduced the experiment that the TMI threshold of the laser increases with the increase of the fiber coiling diameter. Based on this scheme, we achieved a 7 kW laser output.

4. Power Scaling of the Direct LD Pumped Fiber Laser Employing New Suppression Technology

In this section, we will introduce the main results of applying the above new suppression technologies to high-power fiber lasers, including fiber oscillators with an output power of 5–8 kW, near-single-mode fiber amplifiers with an output power of 6 kW, and multimode fiber amplifiers with an output power of more than 20 kW. In addition, there

are narrow linewidth fiber amplifiers with output power exceeding 4 kW and QCW fiber oscillators with peak power exceeding 10 kW. The details are as follows.

4.1. High-Power Fiber Oscillator Based on Pump Wavelength Optimization

In recent years, with the rapid development of fiber grating and other devices, fiber oscillators have made rapid development. In 2012, the output power of all-fiber laser oscillators exceeded 1 kW for the first time [11]. Subsequently, there have been reports of fiber oscillators with output power of several kilowatts. In 2020, Fujikura reported a near-single-mode fiber oscillator (BPP ~0.50 mm-mrad) with an output power of 8 kW [15]. From the existing results, near single-mode fiber oscillator with power exceeding 5 kW has been achieved based on the double cladding YDF with core/cladding diameter of 20/400 μm and the pump source with central wavelength of 976 nm, but there has been obvious SRS, and the power growth is limited [16]. The design of fiber oscillators using double-cladding YDF with a core diameter of 25 μm or 30 μm can suppress SRS, but when using LD with a central wavelength of 976 nm, the laser is limited by TMI, and the larger core diameter also has the problem of maintaining beam quality [93]. Therefore, the scheme based on a larger core diameter combined with pump optimization has the potential to further improve the output power.

4.1.1. WS-981 Bidirectional Pumped 5 kW Fiber Oscillator

We realized a 5 kW near-single-mode ($M^2 < 1.4$) fiber oscillator using double-cladding YDF with a core/cladding diameter of 25/400 μm and WS-981 [94]. The structure of the laser is shown in Figure 13. The reflectivity and 3 dB bandwidth of the high-reflectivity fiber Bragg grating (HRFBG) are 99.8% and 3.92 nm, respectively. The reflectivity and 3 dB bandwidth of the output coupler fiber Bragg grating (OCFBG) are 8.2% and 0.97 nm, respectively. The minimum coiling radius of the active fiber is 4.25 cm to increase the loss of higher-order modes and control the beam quality. The experimental results are shown in Figure 14. Under a bidirectional pump, the maximum output power of the laser is 5120 W. Currently, the corresponding co- and counter-pump powers are 1523 W and 4360 W, respectively, with an efficiency of the laser is 87%. At the maximum output power, there is obvious SRS on the spectrum, and its intensity is about 32.5 dB lower than the signal. The fiber oscillator is continuously operated at the maximum output power for 120 min, and the results are shown in Figure 14b. During the long-term test, the average output power is 5175 W, with a power fluctuation of less than 1%. The beam quality of the laser is always between 1.3 and 1.4, and the beam profile is always good. The intensity of SRS in the spectrum will change with time, but its intensity remains at a level of ~30 dB lower than the signal. The experimental results provide a feasible scheme to realize 5 kW near-single-mode fiber oscillator.

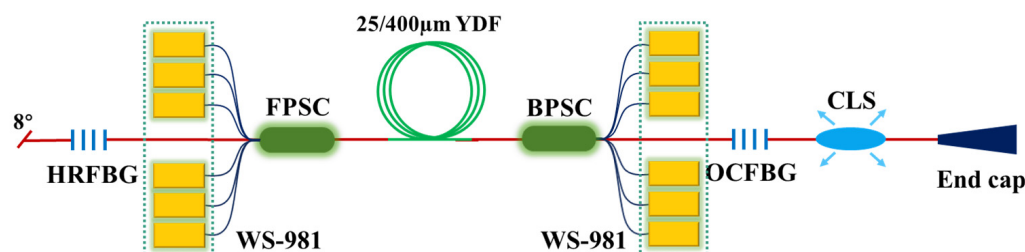


Figure 13. Structure diagram of WS-981 bidirectional pumped 5 kW fiber oscillator.

4.1.2. WS-981 Counter Pumped 8 kW Fiber Oscillator

In the above fiber oscillator based on 25/400 μm fiber, the obvious problem of further power improvement is still the contradiction between TMI and SRS. First, the power improvement of the laser is limited by TMI under the condition of a unidirectional pump. Although the TMI threshold in the counter-pump configuration is higher than that in the co-pump configuration, it is necessary to provide sufficient co-pump power to achieve higher

output power. However, the increase in co-pump power will lead to the rapid enhancement of SRS, and further power scaling is still limited. The realization of higher power needs to balance the SRS and TMI. Therefore, we have designed the laser scheme of WS-981 counter-pumped 30/600 μm YDF, as shown in Figure 15. Compared with conventional 25/400 μm YDF, 30/600 μm YDF has a lower pump absorption coefficient. Combined with WS-981, it can effectively improve the TMI threshold under the unidirectional pump. The fiber core with a diameter of 30 μm combined with the counter-pump configuration can better inhibit SRS. Another improvement of the laser is the use of $(18 + 1) \times 1$ backward pump/signal combiner $((18 + 1) \times 1$ PSC). The core/cladding diameter of the signal input fiber is 30/600 μm , the core/cladding diameter of the signal output fiber is 30/250 μm , and the core/cladding diameter of the pump input fiber is 220/242 μm . This combiner can greatly improve the available pump power of the laser. The grating used in the experiment is self-designed and manufactured. The 3 dB bandwidth of HRFBG and OCFBG is 3.6 nm and 2.0 nm, respectively.

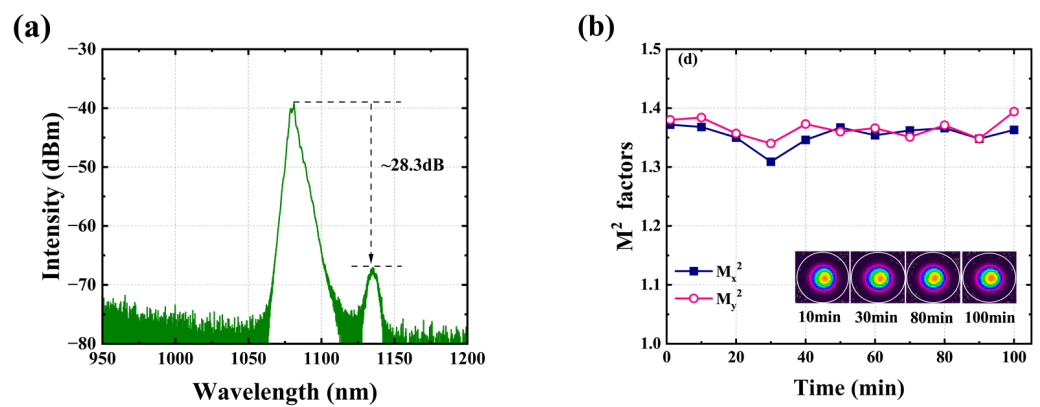


Figure 14. Experimental results of WS-981 bidirectional pumped 5 kW fiber oscillator. (a) Spectrum at the maximum output power; (b) Evolution of M^2 and SRS intensity with time during long operation (inset: beam profile) [94].

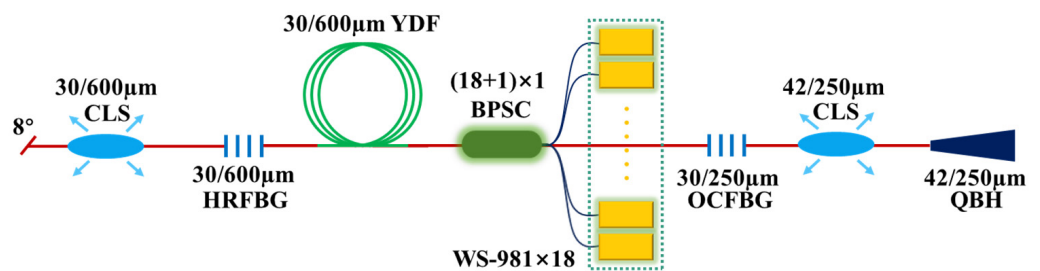


Figure 15. Schematic diagram of the experimental structure of 8 kW fiber laser oscillator.

The experimental results are shown in Figure 16. When the pump power is 10,250 W, the maximum output power is 7920 W, and the conversion efficiency is 77.3%. When the pump power is further increased to 10,350 W, the output power decreases to 7600 W, and the conversion efficiency decreases to 73.4%. Currently, typical TMI characteristics appear in the FFT results of the PD signal. When the output power is 7.5 kW, the spectrum and beam quality of the output laser are shown in Figure 16c,d. No obvious SRS appears and the beam quality M^2 factor is about 2.5 with a brightness of about 1028.8. From the results, the advantages of counter-pump configuration, pump wavelength optimization, and large cladding fiber are fully demonstrated in the experiment. The further development direction of high-power fiber oscillators is the further improvement of power and beam quality.

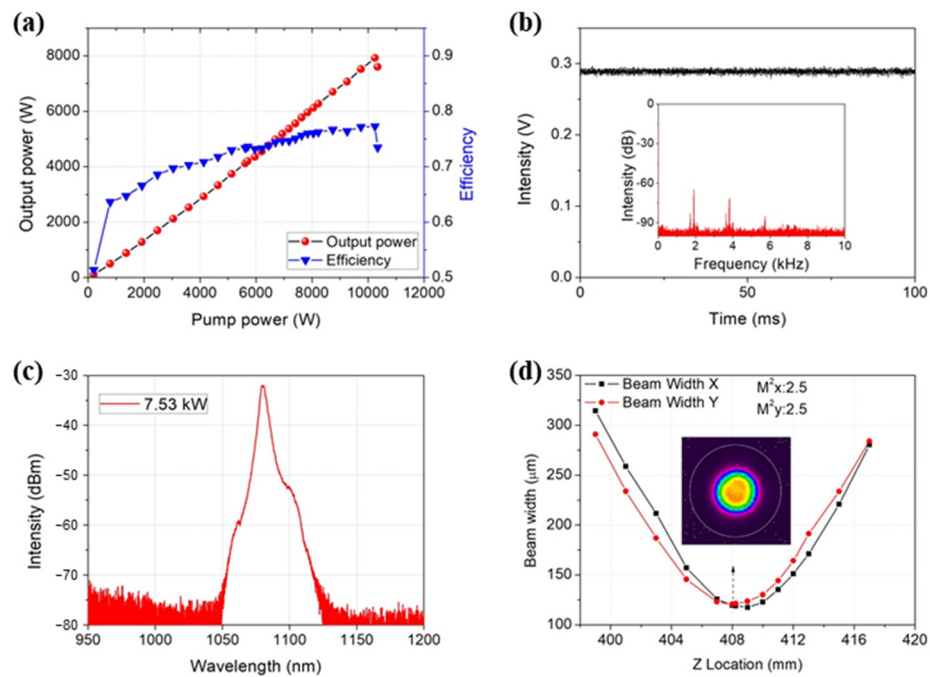


Figure 16. The output results from an 8 kW fiber oscillator. (a) Output power and efficiency at different pump power; (b) Time domain signal and corresponding FFT results when the pump power is 10,350 W and the output power is reduced to 7600 W; (c) The output spectrum at the power of 7.5 kW; (d) The beam quality at the power of 7.5 kW.

4.2. High Power Fiber Amplifier Based on Pump Wavelength Optimization

4.2.1. WS-981 Bidirectional Pumped 6 kW Fiber Amplifier

We realized a 6 kW near-single-mode fiber amplifier [9]. The laser adopts a double-cladding YDF with a core/cladding diameter of 25/400 μm and a length of 19.5 m. In order to suppress TMI, the minimum coiling diameter of the fiber is adjusted to 8 cm. When applying WS-981 for the bidirectional pump, the maximum output power of the laser is 6.01 kW with a slope efficiency of 82.3%. In the bidirectional pump configuration, TMI is suppressed, and SRS becomes the only factor limiting the power scaling. At the maximum output power, the SRS intensity is only 20 dB lower than the signal. The smaller coiling diameter provides better mode control capability for the laser. At 6.01 kW, the beam quality M^2 factor is 1.31 and 1.23 in the x and y directions, respectively.

From the current structure of the laser, under the cladding diameter of 400 μm, the available counter-pump power has reached the limit, so the output power can only be increased by increasing the co-pump. However, the increase of the co-pump will lead to a rapid enhancement of the SRS, and the fiber length of the laser has no potential for optimization. As in the high-power oscillator experiment in Section 4.1, the output power can be further improved by counter-pumping the fiber with a higher TMI threshold.

4.2.2. WS-981 Counter Pumped 7 kW Fiber Amplifier

Based on the analysis in Section 4.2.1, the structure of fiber amplifier capable of achieving higher power is shown in Figure 17. The active fiber of the amplifier adopts double-cladding YDF with core/cladding diameter of 30/600 μm, and the absorption coefficient of the fiber is 0.4 dB/m@915 nm. Combining the above fiber parameters with WS-981, we can predict that the laser has a high TMI threshold. The main amplifier adopts backward pumping mode, and the beam combiner is $(36 + 1) \times 1$ backward pump/signal combiner. The core/cladding diameter of the signal input fiber is 30/600 μm, the core/cladding diameter of the signal output fiber is 30/250 μm, and the core/cladding diameter of the pump input fiber is 135/155 μm. Thirty-six LDs with a maximum output power of about 250 W are used as the pump source of the amplifier. Consistent with the scheme in Section 4.1.2,

the counter-pump configuration combined with a larger core diameter is conducive to SRS suppression and higher output power.

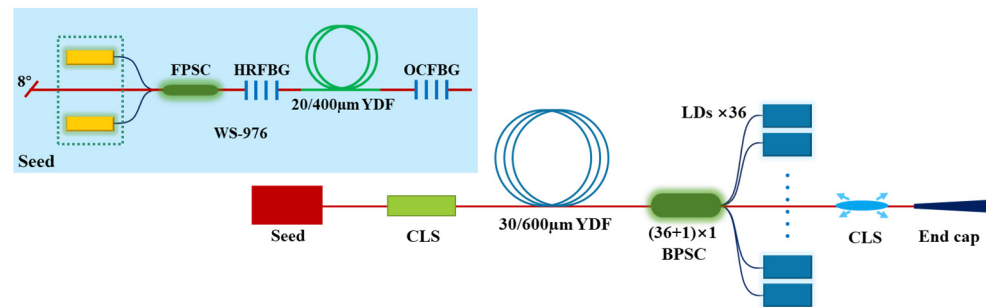


Figure 17. Schematic diagram of experimental structure of 7 kW fiber laser oscillator.

The main results are shown in Figure 18. When all LDs reach the maximum output power, the power of the fiber amplifier is 7020 W. Currently, no SRS appears in the spectrum, and the Stokes intensity at 1135 nm is ~36.7 dB lower than the signal. It shows that a larger core diameter and counter-pump configuration have a significant effect on SRS suppression. At the maximum output power, the beam quality of the laser is $M_x^2 = 1.98$, $M_y^2 = 1.89$. In the experiment, the output characteristics of the laser are compared when the minimum coiling diameter is 12 cm and 11 cm, respectively. The results are shown in Table 7. Reducing the coiling diameter of the fiber will increase the loss of higher-order modes, and ultimately lead to the reduction of laser efficiency and the improvement of beam quality. When the minimum coiling diameter is 12 cm, the maximum output power that can be achieved is 7310 W. However, the beam quality of the output laser is poor. In contrast, when the minimum coiling diameter is 11 cm, the laser has a higher brightness. Since the laser power in the laser is different, the SRS intensity in the output laser is also different under the two coiling diameters.

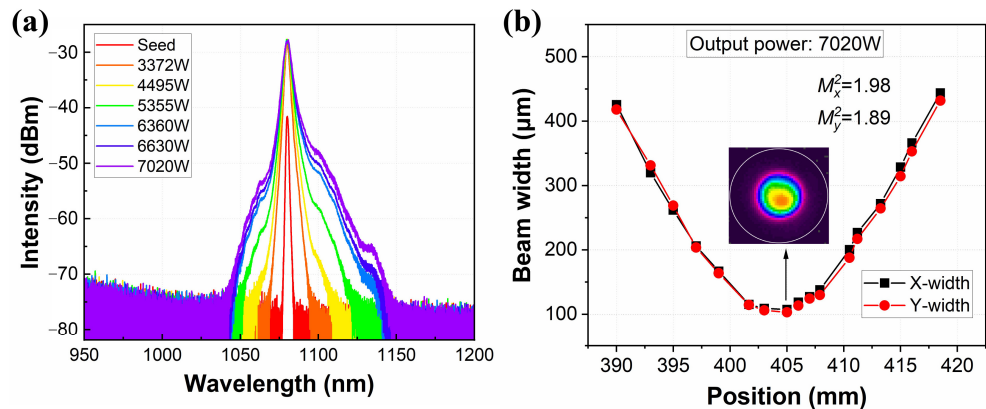


Figure 18. Main results of the 7 kW fiber amplifier. (a) The spectra at different output power; (b) The beam quality at the maximum output power.

Table 7. Comparison of results under different coiling diameters.

Setup	Minimum Coiling Diameter	Maximum Coiling Diameter	Maximum Power	Slope Efficiency	SRS	M ²	Brightness
I	12.0 cm	20.8 cm	7310 W	82.6%	35.3 dB	2.17	1330.9
II	11.0 cm	20.0 cm	7020 W	79.3%	36.7 dB	1.93	1615.8

The feasibility of further improvement of output power can be analyzed from the current laser. First, there is no obvious SRS and TMI in the output results, indicating that

the power can be further improved. The effective way is to increase the available pump power of the laser. In addition, the efficiency and beam quality of the laser can be properly balanced through the control of fiber coiling.

4.2.3. WS-976 Counter Pumped 10 kW Fiber Amplifier by Fiber Coiling Optimization

We realized a 10 kW fiber amplifier based on the self-designed and manufactured low-absorption and low-NA YDF [10]. Consistent with the scheme in the high-power fiber amplifier, the laser applies a counter-pump configuration to suppress SRS. The mode field area of the YDF is about $450 \mu\text{m}^2$, and the core NA is 0.051. The low absorption design of the YDF determines that we can use WS-976 as the pump source. In the experiment, the output power is improved by optimizing the coiling diameter. The schematic diagrams of the two coiling setups are shown in Figure 19. Figure 19a shows the high mode loss coiling setup, with a diameter of 12–24.3 cm. Under this condition, the higher-order mode loss is large, and good beam quality can be obtained. Accordingly, Figure 19b shows the low-mode loss coiling setup with a diameter of 20–28 cm. Under this condition, the higher-order mode loss is small, making it possible to output from the core, and the laser can maintain high efficiency. The comparison of the output results of the laser in the two setups is shown in Table 8. When the coiling setup in Figure 19b is adopted, the maximum output power of the laser reaches 10,530 W with a brightness of 1088.7 without SRS and TMI. All LDs have reached the maximum output power. Therefore, it is possible to further improve the output power and brightness of the laser. It can be seen from the comparison that the TMI threshold of the laser is about 2467 W when the coiling setup with a larger diameter is adopted (Figure 19b), which means that the TMI threshold of the laser decreases with the increase of the coiling diameter of the fiber, which is the same as the conclusion in [72]. This is also a more intuitive abnormal TMI phenomenon in fiber lasers.

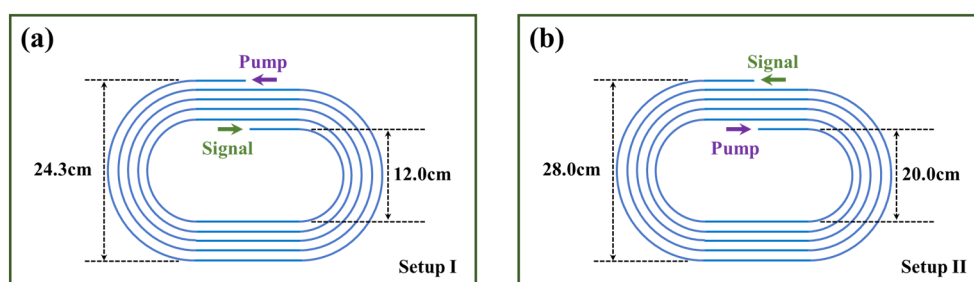


Figure 19. Fiber coiling setup with different mode loss. (a) Coiling setup with high mode loss; (b) coiling setup with low mode loss.

Table 8. Comparison of main results under two coiling setups [10].

Setup	Maximum Power	Efficiency	TMI	SRS	M ²	Brightness	Limiting Factor
I	2543 W	72.64%	2467 W	>40 dB	2.05; 1.91	556.8	TMI
II	10,530 W	74.04%	>10,530 W	30 dB	2.83; 2.93	1088.7	Pump power

4.2.4. WS-981 Counter-Pumped Fiber Amplifiers with Power Exceeding 10 kW

Numerous experiments have verified that the counter-pump configuration combined with the pump wavelength optimization is conducive to the improvement of laser power. The structure of the counter-pumped fiber amplifier is shown in Figure 20. The laser output from the seed enters the amplifier after passing through a mode field adaptor (MFA) and cladding light stripper (CLS). The pump light enters the YDF after passing through a BPSC. The signal light is amplified in the YDF and output from the signal output fiber of the BPSC. In order to improve the available pump power of the laser, the number of pump input fibers or the pump power of each group of LDs should be increased by using the fiber with

a larger cladding diameter. Based on the above ideas, we have successively realized 12 kW and 20 kW high-power fiber amplifiers.

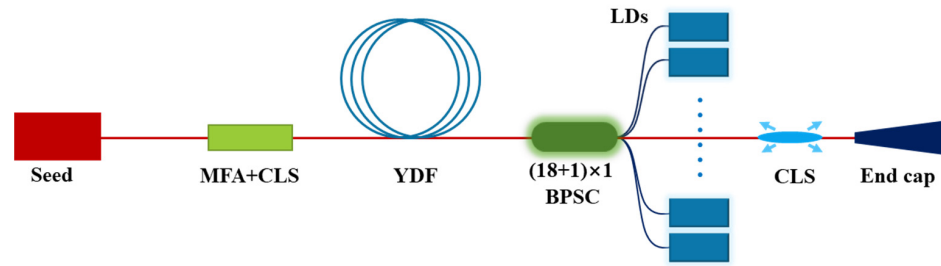


Figure 20. Schematic diagram of the counter-pumped fiber amplifier.

In the 12 kW high-power fiber amplifier, we adopt the YDF with the mode field area of $570 \mu\text{m}^2$ and WS-981. The results are shown in Figure 21. When the seed and pump powers are 100 W and 14.5 kW, respectively, the output power of the laser reaches 12.63 kW. There is no SRS in the spectrum, and the beam quality M^2 factor of the laser is about 2.85. The laser has a brightness of 1333.1. Subsequently, the active fiber is optimized and laser power exceeding 20 kW is realized, as shown in Figure 22. The optimized seed laser power is 510 W. When the pump power is 23.3 kW, the output power is 20.27 kW, and the efficiency is 84.8%. When the output power reaches 15 kW, the beam quality M^2 is about seven. At the maximum output power, the SRS intensity is more than 50 dB lower than the signal. This is the highest power of the LD directly pumped single-channel fiber laser at present. The next step is to carry out mode control and beam quality optimization to improve the brightness of the laser.

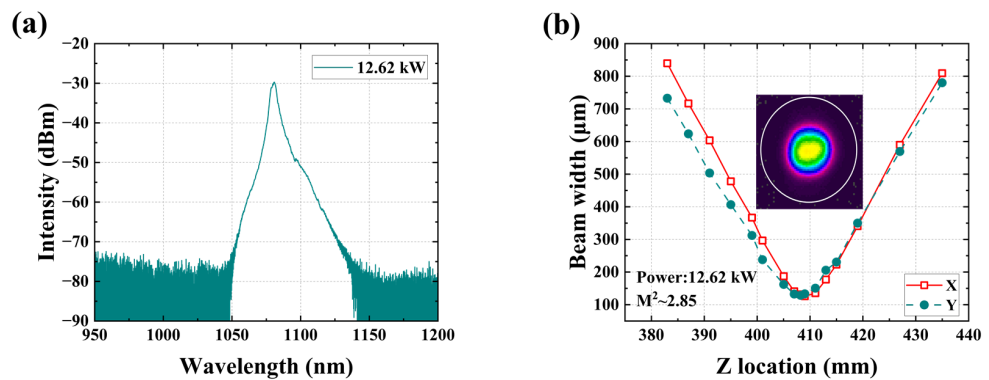


Figure 21. Main results of 12 kW fiber amplifier. (a) Spectrum at the maximum output power; (b) Beam quality at the maximum output power.

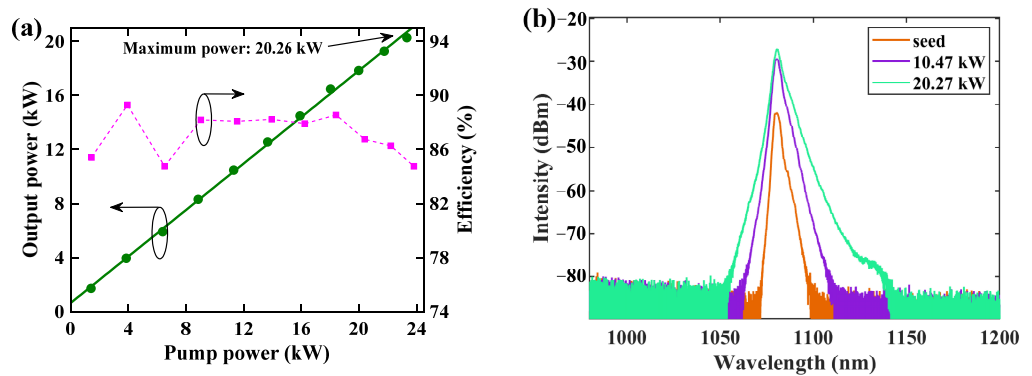


Figure 22. The main results of the counter-pumped 20 kW fiber amplifier. (a) Output power and efficiency at different pump power; (b) Spectra at different output power.

4.3. 4 kW High-Power Counter Pumped Narrow Linewidth Amplifier Based on Pump Wavelength Optimization

Consistent with the wide linewidth CW fiber laser, SRS and TMI are also the limiting factors for the power improvement of narrow linewidth fiber laser. At present, the publicly reported high-power narrow linewidth fiber lasers mostly use bidirectional pump configuration, and there is no realization of more than 4 kW narrow linewidth fiber lasers based on a unidirectional pump [95–97]. Based on the new technical scheme of WS-981 to suppress TMI and counter-pump configuration to suppress SRS, the research group has realized a 4.05 kW single-mode narrow linewidth fiber laser. The structure of the amplifier is shown in Figure 23. The single-frequency seed laser (SF) is injected into the three-level preamplifier (A1, A2, A3) after white noise phase modulation (PM). The white noise signal source (WNS) is used to modulate the phase modulator to broaden the 3 dB linewidth of the seed laser to ~0.6 nm, and then the output power of the seed laser is increased to ~30 W after three stages of pre-amplification. Six groups of LDs with central wavelengths of 976 nm and 981 nm and power of 800 W are injected into the YDF through the $(6 + 1) \times 1$ combiner.

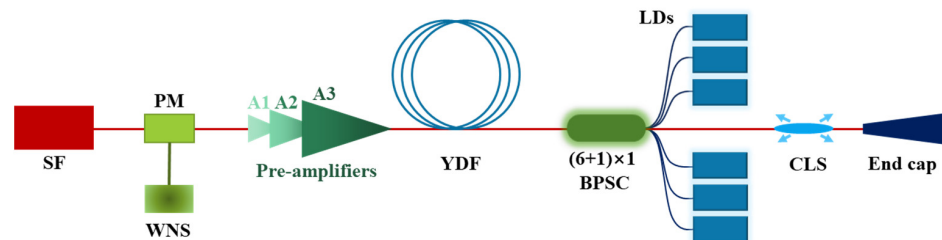


Figure 23. Counter pumped high-power narrow-linewidth fiber amplifier.

The output laser of the amplifier is output after passing through the CLS and the end cap. In the experiment, when the WS-976 is used first, obvious TMI appears when the output power is 3.4 kW. When WS-981 with a total power of 5069 W is used, the output power is 4050 W, and the slope efficiency is 78.2%. At the maximum output power, the 3 dB and 20 dB bandwidths are about 0.60 nm and 1.6 nm, respectively. Obvious SRS appears and the intensity is 40.5 dB lower than the signal, as shown in Figure 24a. As shown in Figure 24b, there is no TMI at the maximum power, and the beam quality is 1.3. Experiments have verified the TMI suppression ability of WS-981 in narrow linewidth amplifiers. By optimizing the laser design and combining it with a bidirectional pump configuration, it is expected to achieve higher-power narrow-linewidth fiber laser output.

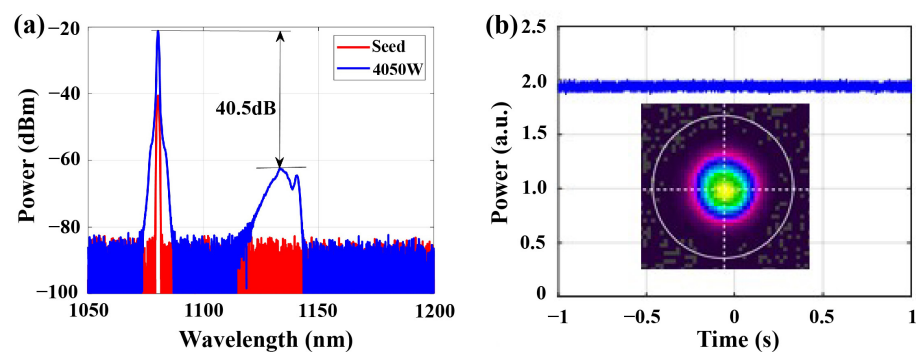


Figure 24. The main experimental results of the counter-pumped high-power narrow-linewidth fiber amplifier. (a) The spectrum of the seed and the laser at maximum output power. (b) PD signal at maximum output power (inset: beam profile of output laser).

4.4. 10 kW QCW Fiber Laser Employing Counter Pump Configuration to Suppression SRS

Quasi-continuous (QCW) fiber laser has a series of advantages, such as high peak power, large pulse energy, low cost, etc. It has emerged in laser cutting, precision welding, special material drilling, additive manufacturing, and other fields. We realized 9713 W

QCW fiber laser based on fiber with a core/cladding diameter of 30/400 μm , but the laser beam quality M^2 is about 2.3 [98]. Subsequently, QCW fiber lasers with peak power of 6.4 kW and 7.3 kW were successively realized in combination with spindle-shaped fiber, and their M^2 was less than 1.5 [99,100]. How to improve the beam quality while improving the peak power, that is, enhancing the brightness, is an important research area. Recently, we have achieved a high-brightness QCW fiber laser oscillator with a peak power exceeding 10 kW and a beam quality (M^2) of 1.61 for the first time. The experiment adopts a counter-pump configuration, as shown in Figure 25. 36 WS-976 are injected into the resonant cavity by customized $(36 + 1) \times 1$ BPSC after square wave modulation. The core/cladding diameters of HRFBG and OCFBG are both 30/400 μm , the central wavelength is 1070 nm, and the reflectivity is 99.5% and 5%, respectively. The gain medium is YDF with an effective mode field area of about 350 μm^2 , and the total absorption coefficient is 11.1 dB in quasi-continuous mode. Under the condition of pump repetition frequency of 1 kHz, QCW laser output with an average output power of 973 W and peak power of 10.75 kW is realized. At the maximum power, the Raman intensity is more than 36 dB lower than the signal, and the conversion efficiency is $\sim 76\%$ (Figure 26a). The beam quality factor (M^2) is 1.61 (Figure 26b), and the brightness is as high as 3555.6, which is the highest brightness of the QCW fiber laser reported publicly. Future work will continue to optimize the fiber parameters to further improve the efficiency, power, and beam quality of the fiber laser.

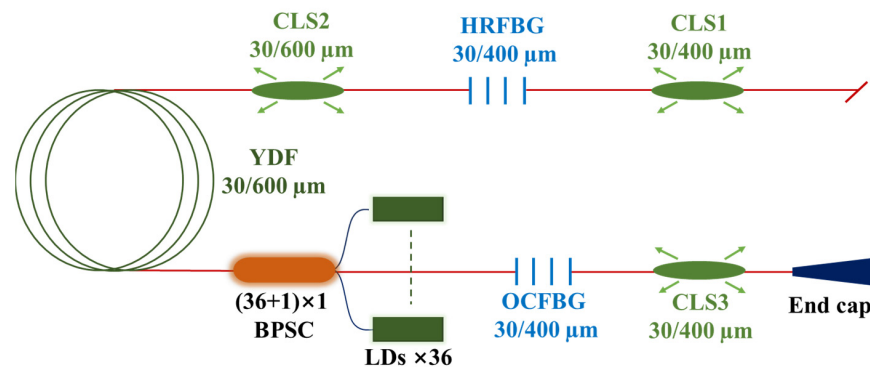


Figure 25. Schematic diagram of the structure of a counter-pumped 10 kW QCW fiber laser.

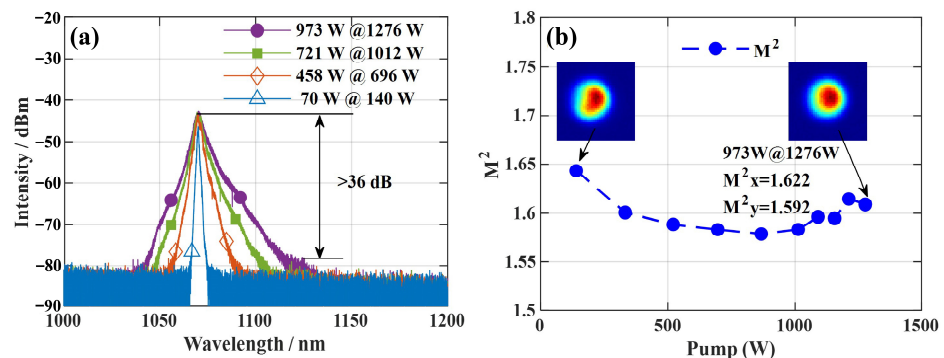


Figure 26. The main results of the 10 kW QCW fiber laser. (a) Spectra at different output power; (b) Beam quality at different pump power.

4.5. Summary

In this section, we introduce high-power fiber oscillators, amplifiers, narrow-linewidth fiber amplifiers, and QCW fiber oscillators based on the new technology. Because the optimized pump wavelength has an obvious inhibitory effect on TMI, we have used the optimized WS-981 as the pump source in most of the above experiments. From the fiber amplifier schemes with different output power, under the condition of sufficient pump power, it is obvious to use the counter-pump configuration as far as possible to suppress SRS. Therefore, the combination of pump wavelength optimization and counter-pump

configuration is a very promising scheme to further improve the laser power. In addition, the counter-pump configuration has significant advantages for narrow linewidth fiber lasers and QCW fiber lasers that are susceptible to nonlinear effects. Subsequent research can also further improve performance by combining pump wavelength optimization and novel fiber.

5. Conclusions

In this article, we focus on the suppression techniques for achieving a balance between SRS and TMI without deteriorating either of them, including fiber coiling optimization, pump wavelength optimization, pump configuration optimization, and novel vary core active fiber. In Sections 2 and 3, the above new technologies and schemes are explained theoretically and verified experimentally in relatively low-power conditions. In Section 4, the typical research results of high-power fiber lasers based on the above measures are introduced. The main results are summarized in Table 9.

Table 9. The main experimental results of high-power fiber lasers are introduced in this paper.

Laser Type	Power	Pump Configuration	Pump Wavelength	M ²	SRS	Brightness
Fiber oscillator	5 kW	Bidirectional pump	WS-981	<1.4	32.5 dB	2187.1
	8 kW	Counter pump	WS-981	2.5	>40 dB	1097.4
Fiber amplifier	6 kW	Bidirectional pump	WS-981	1.27	20 dB	3189.3
	7 kW	Counter pump	WS-981	1.93	36.7 dB	1611.1
	10 kW	Counter pump	WS-976	2.88	30 dB	1088.7
	12 kW	Counter pump	WS-981	2.85	37 dB	1333.1
	20 kW	Counter pump	WS-981	>7	>40 dB	262.4
Narrow-linewidth fiber amplifier	4 kW	Counter pump	WS-981	1.3	40.5 dB	2029.2
QCW fiber oscillator	Peak 10 kW	Counter pump	WS-976	1.61	36 dB	3555.6

The pump configuration optimization, pump wavelength optimization and fiber coiling optimization are widely used in the above experiments. All applications are based on balancing the suppression of SRS and TMI. At present, the maximum average output power of fiber laser based on VCAF is 6 kW. In the follow-up study, VCAF can be combined with the above mature methods. The realization of direct LD-pumped fiber lasers with higher output power must also consider the above new technical schemes. Benefiting from a balance between SRS and TMI, the counter-pump configuration is expected to become the mainstream scheme in the follow-up high-power fiber lasers. However, it is necessary to match the backward pump and signal combiner that can withstand higher power and the LDs with higher power and brightness. The suppression of an abnormal TMI based on fiber coiling optimization provides another new way to achieve higher power. With the development of various technologies, we believe that the comprehensive application of the above new technical solutions can bring the output performance (power, spectrum, and brightness) of fiber lasers to a higher level.

Author Contributions: Conceptualization, X.W. and X.X. (Xiaojun Xu); methodology, X.W., C.S., B.Y., P.W. and X.X. (Xiaoming Xi); software, C.S., Y.Y. and L.Z.; validation, B.Y., Y.Y., L.Z., Z.P. and L.W.; formal analysis, K.H., H.Z. and X.X. (Xiaojun Xu); investigation, X.W., C.S. and H.Z.; resources, X.W., L.Z., Y.Y., L.W. and B.Y.; data curation, Y.Y. and L.Z.; writing—original draft preparation, L.Z. and X.W.; writing—review and editing, X.W. and X.X. (Xiaoming Xi); visualization, Y.Y. and L.W.; supervision, P.W., H.Z. and X.X. (Xiaoming Xi); project administration, X.X. (Xiaoming Xi), X.W. and H.Z.; funding acquisition, X.W., K.H. and X.X. (Xiaojun Xu). All authors have read and agreed to the published version of the manuscript.

Funding: This work is supported by Funds for Distinguished Youth of Hunan Province (2023JJ10057), Training Program for Excellent Young Innovations of Changsha (kq2206006) and Basic Scientific Research Program (JCKY2021525B015).

Institutional Review Board Statement: Not applicable.

Informed Consent Statement: Not applicable.

Data Availability Statement: Not applicable.

Conflicts of Interest: The authors declare no conflict of interest.

References

1. Jeong, Y.; Sahu, J.; Payne, D.; Nilsson, J. Ytterbium-doped large-core fiber laser with 1.36 kW continuous-wave output power. *Opt. Express* **2004**, *12*, 6088–6092. [[CrossRef](#)]
2. Gapontsev, V.; Gapontsev, D.; Platonov, N.; Shkurikhin, O.; Ferin, S. 2 kW CW ytterbium fiber laser with record diffraction-limited brightness. In Proceedings of the Conference on Lasers & Electro-Optics Europe, Munich, Germany, 12–17 June 2005.
3. Yu, H.; Zhang, H.; Lv, H.; Wang, X.; Leng, J.; Xiao, H.; Guo, S.; Zhou, P.; Xu, X.; Chen, J. 3.15 kW direct diode-pumped near diffraction-limited all-fiber-integrated fiber laser. *Appl. Opt.* **2015**, *54*, 4556–4560. [[CrossRef](#)] [[PubMed](#)]
4. Fang, Q.; Li, J.; Shi, W.; Qin, Y.; Xu, Y.; Meng, X.; Norwood, R.A.; Peyghambarian, N. 5 kW Near-Diffraction-Limited and 8 kW High-Brightness Monolithic Continuous Wave Fiber Lasers Directly Pumped by Laser Diodes. *IEEE Photonics J.* **2017**, *9*, 1–7. [[CrossRef](#)]
5. Wang, Y.; Gao, C.; Tang, X.; Zhan, H.; Peng, K.; Ni, L.; Liu, S.; Li, Y.; Guo, C.; Wang, X.; et al. 30/900 Yb-doped Aluminophosphosilicate Fiber Presenting 6.85-kW Laser Output Pumped With Commercial 976-nm Laser Diodes. *J. Light. Technol.* **2018**, *36*, 3396–3402. [[CrossRef](#)]
6. Beier, F.; Möller, F.; Sattler, B.; Nold, J.; Liem, A.; Hupel, C.; Kuhn, S.; Hein, S.; Haarlammert, N.; Schreiber, T.; et al. Experimental investigations on the TMI thresholds of low-NA Yb-doped single-mode fibers. *Opt. Lett.* **2018**, *43*, 1291–1294. [[CrossRef](#)]
7. Lin, H.; Xu, L.; Li, C.; Shu, Q.; Chu, Q.; Xie, L.; Guo, C.; Zhao, P.; Li, Z.; Wang, J.; et al. 10.6 kW high-brightness cascade-end-pumped monolithic fiber lasers directly pumped by laser diodes in step-index large mode area double cladding fiber. *Results Phys.* **2019**, *14*, 102479. [[CrossRef](#)]
8. Wu, H.; Li, R.; Xiao, H.; Huang, L.; Yang, H.; Pan, Z.; Leng, J.; Zhou, P. High-power tandem-pumped fiber amplifier with beam quality maintenance enabled by the confined-doped fiber. *Opt. Express* **2021**, *29*, 31337. [[CrossRef](#)] [[PubMed](#)]
9. Yang, B.; Wang, P.; Zhang, H.; Xi, X.; Shi, C.; Wang, X.; Xu, X. 6 kW single mode monolithic fiber laser enabled by effective mitigation of the transverse mode instability. *Opt. Express* **2021**, *29*, 26366. [[CrossRef](#)]
10. Wen, Y.; Wang, P.; Xi, X.; Zhang, H.; Huang, L.; Yang, H.; Yan, Z.; Yang, B.; Shi, C.; Pan, Z.; et al. LD Direct Counter-Pumped 10 kW Fiber Laser Amplifier With Good Beam Quality. *Acta Phys. Sin.-Ch. Ed.* **2022**, *71*, 244202. [[CrossRef](#)]
11. Xiao, Y.; Brunet, F.; Kanskar, M.; Faucher, M.; Wetter, A.; Holehouse, N. 1-kilowatt CW all-fiber laser oscillator pumped with wavelength-beam-combined diode stacks. *Opt. Express* **2012**, *20*, 3296–3301. [[CrossRef](#)] [[PubMed](#)]
12. Yang, B.; Zhang, H.; Shi, C.; Wang, X.; Zhou, P.; Xu, X.; Chen, J.; Liu, Z.; Lu, Q. Mitigating transverse mode instability in all-fiber laser oscillator and scaling power up to 2.5 kW employing bidirectional-pump scheme. *Opt. Express* **2016**, *24*, 27828–27835. [[CrossRef](#)] [[PubMed](#)]
13. Ackermann, M.; Rehmann, G.; Lange, R.; Witte, U.; Safarzadeh, F.; Boden, B.; Weber, H.; Netz, D.; Perne, C.; Kösters, A.; et al. Extraction of more than 10 kW from a single ytterbium-doped MM-fiber. In *Fiber Lasers XVI: Technology and Systems*; SPIE: San Francisco, CA, USA, 2019.
14. Ye, Y.; Yang, B.; Wang, P.; Zeng, L.; Xi, X.; Shi, C.; Zhang, H.; Wang, X.; Zhou, P.; Xu, X. Industrial 6 kW high-stability single-stage all-fiber laser oscillator based on conventional large mode area ytterbium-doped fiber. *Laser Phys.* **2021**, *31*, 35104. [[CrossRef](#)]
15. Wang, Y.; Rintaro, K.; Kiyoyama, W.; Shirakura, Y.; Kurihara, T.; Nakanishi, Y.; Yamamoto, T.; Nakayama, M.; Ikoma, S.; Shima, K. 8-kW single-stage all-fiber Yb-doped fiber laser with a BPP of 0.50 mm-mrad. In *Fiber Lasers XVII: Technology and Systems*; SPIE: San Francisco, CA, USA, 2020.
16. Krmer, R.G.; Miller, F.; Matzdorf, C.; Goebel, T.A.; Nolte, S. Extremely robust femtosecond written fiber Bragg gratings for ytterbium doped fiber oscillator with 5 kW output power. *Opt. Lett.* **2020**, *45*, 1447–1450. [[CrossRef](#)] [[PubMed](#)]
17. Zervas, M.N.; Codemard, C.A. High Power Fiber Lasers: A Review. *IEEE J. Sel. Top. Quant.* **2014**, *20*, 219–241. [[CrossRef](#)]
18. Beyer, E.; Mahrle, A.; Lütke, M.; Standfuss, J.; Brückner, F. Innovations in high power fiber laser applications. In *Fiber Lasers IX: Technology, Systems, and Applications*; SPIE: San Francisco, CA, USA, 2012.
19. Zervas, M.N. Transverse mode instability, thermal lensing and power scaling in Yb³⁺-doped high-power fiber amplifiers. *Opt. Express* **2019**, *27*, 19019–19041. [[CrossRef](#)]
20. Jauregui, C.; Stihler, C.; Limpert, J. Transverse mode instability. *Adv. Opt. Photonics* **2020**, *12*, 429–484. [[CrossRef](#)]
21. Eidam, T.; Hanf, S.; Seise, E.; Andersen, T.V.; Gabler, T.; Wirth, C.; Schreiber, T.; Limpert, J.; Tunnermann, A. Femtosecond fiber CPA system emitting 830 W average output power. *Opt. Lett.* **2010**, *35*, 94–96. [[CrossRef](#)]
22. Stutzki, F.; Otto, H.J.; Jansen, F.; Gaida, C.; Jauregui, C.; Limpert, J.; Tunnermann, A. High-speed modal decomposition of mode instabilities in high-power fiber lasers. *Opt. Lett.* **2011**, *36*, 4572–4574. [[CrossRef](#)]

23. Stutzki, F.; Jansen, F.; Eidam, T.; Steinmetz, A.; Jauregui, C.; Limpert, J.; Tünnermann, A. High average power large-pitch fiber amplifier with robust single-mode operation. *Opt. Lett.* **2011**, *36*, 689. [[CrossRef](#)]
24. Smith, A.V.; Smith, J.J. Mode instability in high power fiber amplifiers. *Opt. Express* **2011**, *19*, 10180–10192. [[CrossRef](#)]
25. Jauregui, C.; Eidam, T.; Limpert, J.; Tünnermann, A. The impact of modal interference on the beam quality of high-power fiber amplifiers. *Opt. Express* **2011**, *19*, 3258–3271. [[CrossRef](#)]
26. Eidam, T.; Wirth, C.; Jauregui, C.; Stutzki, F.; Jansen, F.; Otto, H.; Schmidt, O.; Schreiber, T.; Limpert, J.; Tünnermann, A. Experimental observations of the threshold-like onset of mode instabilities in high power fiber amplifiers. *Opt. Express* **2011**, *19*, 13218–13224. [[CrossRef](#)] [[PubMed](#)]
27. Hansen, K.R.; Alkeskjold, T.T.; Broeng, J.; Laegsgaard, J. Thermally induced mode coupling in rare-earth doped fiber amplifiers. *Opt. Lett.* **2012**, *37*, 2382–2384. [[CrossRef](#)] [[PubMed](#)]
28. Jansen, F.; Stutzki, F.; Otto, H.; Eidam, T.; Liem, A.; Jauregui, C.; Limpert, J.; Tünnermann, A. Thermally induced waveguide changes in active fibers. *Opt. Express* **2012**, *20*, 3997–4008. [[CrossRef](#)]
29. Jauregui, C.; Eidam, T.; Otto, H.; Stutzki, F.; Jansen, F.; Limpert, J.; Tünnermann, A. Physical origin of mode instabilities in high-power fiber laser systems. *Opt. Express* **2012**, *20*, 12912–12925. [[CrossRef](#)] [[PubMed](#)]
30. Ward, B.; Robin, C.; Dajani, I. Origin of thermal modal instabilities in large mode area fiber amplifiers. *Opt. Express* **2012**, *20*, 11407–11422. [[CrossRef](#)]
31. Beier, F.; Hupel, C.; Kuhn, S.; Hein, S.; Nold, J.; Proske, F.; Sattler, B.; Liem, A.; Jauregui, C.; Limpert, J.; et al. Single mode 4.3 kW output power from a diode-pumped Yb-doped fiber amplifier. *Opt. Express* **2017**, *25*, 14892–14899. [[CrossRef](#)] [[PubMed](#)]
32. Yu, C.X.; Shatrovov, O.; Fan, T.Y.; Taunay, T.F. Diode-pumped narrow linewidth multi-kilowatt metalized Yb fiber amplifier. *Opt. Lett.* **2016**, *41*, 5202–5205. [[CrossRef](#)] [[PubMed](#)]
33. Dong, L.; Peng, X.; Li, J. Leakage channel optical fibers with large effective area. *J. Opt. Soc. Am. B* **2007**, *24*, 1689–1697. [[CrossRef](#)]
34. Gu, G.; Kong, F.; Hawkins, T.; Parsons, J.; Jones, M.; Dunn, C.; Kalichevsky-Dong, M.T.; Saitoh, K.; Dong, L. Ytterbium-doped large-mode-area all-solid photonic bandgap fiber lasers. *Opt. Express* **2014**, *22*, 13962–13968. [[CrossRef](#)] [[PubMed](#)]
35. Ma, X.; Zhu, C.; Hu, I.; Kaplan, A.; Galvanauskas, A. Single-mode chirally-coupled-core fibers with larger than 50 μm diameter cores. *Opt. Express* **2014**, *22*, 9206–9219. [[CrossRef](#)] [[PubMed](#)]
36. Laurila, M.; Jørgensen, M.M.; Hansen, K.R.; Alkeskjold, T.T.; Broeng, J.; Lægsgaard, J. Distributed mode filtering rod fiber amplifier delivering 292W with improved mode stability. *Opt. Express* **2012**, *20*, 5742–5753. [[CrossRef](#)] [[PubMed](#)]
37. Sanjabi, E.Z.; Antonio-Lopez, J.E.; Anderson, J.; Schulzgen, A.; Amezcua-Correa, R. Reduced-symmetry LMA rod-type fiber for enhanced higher-order mode delocalization. *Opt. Lett.* **2017**, *42*, 1974–1977. [[CrossRef](#)] [[PubMed](#)]
38. Marciante, J.R. Gain Filtering for Single-Spatial-Mode Operation of Large-Mode-Area Fiber Amplifiers. *IEEE J. Sel. Top. Quant.* **2009**, *15*, 30–36. [[CrossRef](#)]
39. Kokki, T.; Koponen, J.; Laurila, M.; Ye, C. Fiber amplifier utilizing an Yb-doped large-mode-area fiber with confined doping and tailored refractive index profile. In *Fiber Lasers VII: Technology, Systems, and Applications*; SPIE: San Francisco, CA, USA, 2010; pp. 758016–758019.
40. Marciante, J.R.; Roides, R.G.; Shkunov, V.V.; Rockwell, D.A. Near-diffraction-limited operation of step-index large-mode-area fiber lasers via gain filtering. *Opt. Lett.* **2010**, *35*, 1828–1830. [[CrossRef](#)]
41. Liao, L.; Zhang, F.; He, X.; Chen, Y.; Wang, Y.; Li, H.; Peng, J.; Yang, L.; Dai, N.; Li, J. Confined-doped fiber for effective mode control fabricated by MCVD process. *Appl. Opt. Technol. Biomed. Opt.* **2018**, *57*, 3244–3249. [[CrossRef](#)]
42. Zhang, F.; Wang, Y.; Lin, X.; Cheng, Y.; Zhang, Z.; Liu, Y.; Li, J. Gain-tailored Yb/Ce codoped aluminosilicate fiber for laser stability improvement at high output power. *Opt. Express* **2019**, *27*, 20824–20836. [[CrossRef](#)]
43. Huang, Z.; Shu, Q.; Luo, Y.; Tao, R.; Feng, X.; Liu, Y.; Lin, H.; Wang, J.; Jing, F. 3.5 kW narrow-linewidth monolithic fiber amplifier at 1064 nm by employing a confined doping fiber. *J. Opt. Soc. Am. B* **2021**, *38*, 2945–2952. [[CrossRef](#)]
44. Jetschke, S.; Unger, S.; Schwuchow, A.; Leich, M.; Kirchhof, J. Efficient Yb laser fibers with low photodarkening by optimization of the core composition. *Opt. Express* **2008**, *16*, 15540–15545. [[CrossRef](#)]
45. Jauregui, C.; Stutzki, F.; Tünnermann, A.; Limpert, J. Thermal analysis of Yb-doped high-power fiber amplifiers with Al:P co-doped cores. *Opt. Express* **2018**, *26*, 7614–7624. [[CrossRef](#)]
46. Jetschke, S.; Unger, S.; Schwuchow, A.; Leich, M.; Jäger, M. Role of Ce in Yb/Al laser fibers: Prevention of photodarkening and thermal effects. *Opt. Express* **2016**, *24*, 13009–13022. [[CrossRef](#)]
47. Hochheim, S.; Brockmüller, E.; Wessels, P.; Koponen, J.; Lowder, T.; Novotny, S.; Willke, B.; Neumann, J.; Kracht, D. Single-Frequency 336 W Spliceless All-Fiber Amplifier Based on a Chirally-Coupled-Core Fiber for the Next Generation of Gravitational Wave Detectors. *J. Light. Technol.* **2022**, *40*, 2136–2143. [[CrossRef](#)]
48. Yuan, M.; Sui, Y.; Bai, Z.; Fan, Z. Recent Advances in Chirally-Coupled Core Fibers. *Front. Phys.* **2022**, *10*, 950492. [[CrossRef](#)]
49. Smith, A.V.; Smith, J.J.; Ramachandran, S. Raising the mode instability thresholds of fiber amplifiers. In *Fiber Lasers XI: Technology, Systems, and Applications*; SPIE: San Francisco, CA, USA, 2014.
50. Beier, F.; Hupel, C.; Nold, J.; Kuhn, S.; Hein, S.; Ihring, J.; Sattler, B.; Haarlammert, N.; Schreiber, T.; Eberhardt, R.; et al. Narrow linewidth, single mode 3 kW average power from a directly diode pumped ytterbium-doped low NA fiber amplifier. *Opt. Express* **2016**, *24*, 6011–6020. [[CrossRef](#)]
51. Tao, R.; Su, R.; Ma, P.; Wang, X.; Zhou, P. Suppressing mode instabilities by optimizing the fiber coiling methods. *Laser Phys. Lett.* **2016**, *14*, 25101. [[CrossRef](#)]

52. Zhu, S.; Li, J.; Li, L.; Sun, K.; Hu, C.; Shao, X.; Ma, X. Mode instabilities in Yb:YAG crystalline fiber amplifiers. *Opt. Express* **2019**, *27*, 35065–35078. [[CrossRef](#)] [[PubMed](#)]
53. Jauregui, C.; Otto, H.; Stutzki, F.; Jansen, F.; Limpert, J.; Tünnermann, A. Passive mitigation strategies for mode instabilities in high-power fiber laser systems. *Opt. Express* **2013**, *21*, 19375–19386. [[CrossRef](#)] [[PubMed](#)]
54. Brar, K.; Savage-Leuchs, M.; Henrie, J.; Courtney, S.; Dilley, C.; Afzal, R.; Honea, E.; Ramachandran, S. Threshold power and fiber degradation induced modal instabilities in high-power fiber amplifiers based on large mode area fibers. In *Fiber Lasers XI: Technology, Systems, and Applications*; SPIE: San Francisco, CA, USA, 2014; p. 89611R.
55. Hejaz, K.; Norouzey, A.; Poozesh, R.; Heidariazar, A.; Roohforouz, A.; Rezaei Nasirabad, R.; Tabatabaei Jafari, N.; Hamedani Golshan, A.; Babazadeh, A.; Lafouti, M. Controlling mode instability in a 500 W ytterbium-doped fiber laser. *Laser Phys.* **2014**, *24*, 25102. [[CrossRef](#)]
56. Tao, R.; Ma, P.; Wang, X.; Zhou, P.; Liu, Z. Study of wavelength dependence of mode instability based on a semi-analytical model. *IEEE J. Quantum Elect.* **2015**, *51*, 1600106.
57. Tao, R.; Ma, P.; Wang, X.; Zhou, P.; Liu, Z. Mitigating of modal instabilities in linearly-polarized fiber amplifiers by shifting pump wavelength. *J. Opt.* **2015**, *17*, 45504. [[CrossRef](#)]
58. Otto, H.; Modsching, N.; Jauregui, C.; Limpert, J.; Tünnermann, A.; Shaw, L.B. Wavelength dependence of maximal diffraction-limited output power of fiber lasers. In *Advanced Solid State Lasers 2014*; SPIE: Shanghai, China, 2015; p. 93441Y.
59. Yang, B.; Zhang, H.; Wang, X.; Su, R.; Tao, R.; Zhou, P.; Xu, X.; Lu, Q. Mitigating transverse mode instability in a single-end pumped all-fiber laser oscillator with a scaling power of up to 2 kW. *J. Opt.* **2016**, *18*, 105803. [[CrossRef](#)]
60. Jauregui, C.; Otto, H.; Breikopf, S.; Limpert, J.; Tünnermann, A. Optimizing high-power Yb-doped fiber amplifier systems in the presence of transverse mode instabilities. *Opt. Express* **2016**, *24*, 7879–7892. [[CrossRef](#)] [[PubMed](#)]
61. Wan, Y.; Xi, X.; Yang, B.; Zhang, H.; Wang, X. Enhancement of TMI Threshold in Yb-Doped Fiber Laser by Optimizing Pump Wavelength. *IEEE Photonics Tech. Lett.* **2021**, *33*, 656–659. [[CrossRef](#)]
62. Wan, Y.; Yang, B.; Xi, X.; Zhang, H.; Wang, P.; Wang, X.; Xu, X. Comparison and Optimization on Transverse Mode Instability of Fiber Laser Amplifier Pumped by Wavelength-Stabilized and Non-Wavelength-Stabilized 976 nm Laser Diode. *IEEE Photonics J.* **2022**, *14*, 1503905. [[CrossRef](#)]
63. Rezaei-Nasirabad, R.; Azizi, S.; Paygan, D.; Tavassoli, M.; Abedinajafi, A.; Roohforouz, A.; Chenar, R.E.; Golshan, A.H.; Hejaz, K.; Vatani, V. 2.5 kW TMI-free co-pump Yb-doped fiber oscillator by 971.5 nm pumping wavelength. *Opt. Laser Technol.* **2023**, *157*, 108652. [[CrossRef](#)]
64. Naderi, S.; Dajani, I.; Grosek, J.; Madden, T.; Dinh, T.; Vodopyanov, K.L. Theoretical analysis of effect of pump and signal wavelengths on modal instabilities in Yb-doped fiber amplifiers. In *Nonlinear Frequency Generation and Conversion: Materials, Devices, and Applications XIII*; SPIE: San Francisco, CA, USA, 2014.
65. Otto, H.; Jauregui, C.; Stutzki, F.; Jansen, F.; Limpert, J.; Tünnermann, A. Controlling mode instabilities by dynamic mode excitation with an acousto-optic deflector. *Opt. Express* **2013**, *21*, 17285–17298. [[CrossRef](#)]
66. Jauregui, C.; Stihler, C.; Tünnermann, A.; Limpert, J. Pump-modulation-induced beam stabilization in high-power fiber laser systems above the mode instability threshold. *Opt. Express* **2018**, *26*, 10691–10704. [[CrossRef](#)]
67. Lægsgaard, J. Static thermo-optic instability in double-pass fiber amplifiers. *Opt. Express* **2016**, *24*, 13429–13443. [[CrossRef](#)]
68. Montoya, J.; Hwang, C.; Martz, D.; Aleshire, C.; Fan, T.Y.; Ripin, D.J. Photonic lantern kW-class fiber amplifier. *Opt. Express* **2017**, *25*, 27543–27550. [[CrossRef](#)] [[PubMed](#)]
69. Zhou, P.; Xiao, H.; Leng, J.; Xu, J.; Chen, Z.; Zhang, H.; Liu, Z. High-power fiber lasers based on tandem pumping. *J. Opt. Soc. Am. B* **2017**, *34*, A29–A36. [[CrossRef](#)]
70. Li, R.; Wu, H.; Xiao, H.; Leng, J.; Zhou, P. More than 5 kW counter tandem pumped fiber amplifier with near single-mode beam quality. *Opt. Laser Technol.* **2022**, *153*, 108204. [[CrossRef](#)]
71. Wu, H.; Song, J.; Ma, P.; Liu, W.; Ren, S.; Wang, G.; Li, R.; Xiao, H.; Huang, L.; Leng, J.; et al. Bidirectional tandem-pumped high-brightness 6 kW level narrow-linewidth confined-doped fiber amplifier exploiting the side-coupled technique. *Opt. Express* **2022**, *30*, 21338–21348. [[CrossRef](#)]
72. Wen, Y.; Wang, P.; Shi, C.; Yang, B.; Xi, X.; Zhang, H.; Wang, X. Experimental Study on Transverse Mode Instability Characteristics of Few-Mode Fiber Laser Amplifier Under Different Bending Conditions. *IEEE Photonics J.* **2022**, *14*, 1539106. [[CrossRef](#)]
73. Zeng, L.; Xi, X.; Ye, Y.; Zhang, H.; Wang, X.; Pan, Z.; Wang, Z.; Xu, X. Near-single-mode 3 kW monolithic fiber oscillator based on a longitudinally spindle-shaped Yb-doped fiber. *Opt. Lett.* **2020**, *45*, 5792–5795. [[CrossRef](#)] [[PubMed](#)]
74. Zeng, L.; Xi, X.; Ye, Y.; Lin, X.; Wang, X.; Li, J.; Shi, C.; Yang, B.; Zhang, H.; Wang, P.; et al. A novel fiber laser oscillator employing saddle-shaped core ytterbium-doped fiber. *Appl. Phys. B* **2020**, *126*, 185. [[CrossRef](#)]
75. Ye, Y.; Lin, X.; Yang, B.; Xi, X.; Shi, C.; Zhang, H.; Wang, X.; Li, J.; Xu, X. Tapered Yb-doped fiber enabled a 4 kW near-single-mode monolithic fiber amplifier. *Opt. Lett.* **2022**, *47*, 2162–2165. [[CrossRef](#)]
76. Ye, Y.; Lin, X.; Xi, X.; Zhang, H.; Yang, B.; Shi, C.; Wang, X.; Li, J.; Xu, X. Demonstration of constant-cladding tapered-core Yb-doped fiber for mitigating thermally-induced mode instability in high-power monolithic fiber amplifiers. *Opt. Express* **2022**, *30*, 24936–24947. [[CrossRef](#)] [[PubMed](#)]
77. Ye, Y.; Lin, X.; Xi, X.; Zhang, H.; Wang, X.; Li, J.; Xu, X. Large mode area saddle-shaped core Yb-doped fiber enabled monolithic high-power, high-efficiency, near-diffraction-limited MOPA laser. In Proceedings of the Thirteenth International Conference on Information Optics and Photonics (CIOP 2022), Xi'an, China, 7–10 August 2022.

78. Ye, Y.; Lin, X.; Xi, X.; Shi, C.; Yang, B.; Zhang, H.; Wang, X.; Li, J.; Xu, X. Novel constant-cladding tapered-core ytterbium-doped fiber for high-power fiber laser oscillator. *High Power Laser Sci.* **2021**, *9*, 142–148. [[CrossRef](#)]
79. Zeng, L.; Pan, Z.; Xi, X.; Yang, H.; Ye, Y.; Huang, L.; Zhang, H.; Wang, X.; Wang, Z.; Zhou, P.; et al. 5 kW monolithic fiber amplifier employing homemade spindle-shaped ytterbium-doped fiber. *Opt. Lett.* **2021**, *46*, 1393–1396. [[CrossRef](#)]
80. Lin, X.; Ye, Y.; Zhang, Z.; Wang, X.; Xing, Y.; Chen, G.; Peng, J.; Li, H.; Dai, N.; Li, J. 2.7 kW co-pumped fiber amplifier based on constant-cladding tapered-core fiber. *Opt. Fiber Technol.* **2022**, *68*, 102773. [[CrossRef](#)]
81. Zhang, Z.; Lin, X.; Zhang, X.; Luo, Y.; Liao, S.; Wang, X.; Chen, G.; Xing, Y.; Li, H.; Peng, J.; et al. Low-numerical aperture confined-doped long-tapered Yb-doped silica fiber for a single-mode high-power fiber amplifier. *Opt. Express* **2022**, *30*, 32333–32346. [[CrossRef](#)]
82. Glass, A.; Goodwin, E.; Trenholme, J. Characterization of optical nonlinearity in transparent dielectrics and implications for fusion laser design. *IEEE J. Quantum Elect.* **1975**, *11*, 850–851. [[CrossRef](#)]
83. Perry, M.D.; Ditmire, T.; Stuart, B.C. Self-phase modulation in chirped-pulse amplification. *Opt. Lett.* **1994**, *19*, 2149–2151. [[CrossRef](#)]
84. Smith, A.V.; Smith, J.J. *Maximizing the Mode Instability Threshold of a Fiber Amplifier*; Cornell University: Ithaca, NY, USA, 2013.
85. Wan, Y.; Yang, B.; Wang, P.; Xi, X.; Zhang, H.; Wang, X. Optimizing the pump wavelength to improve the transverse mode instability threshold of fiber laser by 3.45 times. *J. Mod. Optic.* **2021**, *68*, 967–974. [[CrossRef](#)]
86. Li, J.; Wang, J.; Jing, F. Improvement of Coiling Mode to Suppress Higher-Order-Modes by Considering Mode Coupling for Large-Mode-Area Fiber Laser. *J. Electromagnet. Wave.* **2010**, *24*, 1113–1124. [[CrossRef](#)]
87. Chu, Q.; Tao, R.; Lin, H.; Wang, J.; Jing, F. Impact of bend-induced mode distortion on mode instability in high power fiber amplifiers. In Proceedings of the Sixth Symposium on Novel Optoelectronic Detection Technology and Applications, Beijing, China, 3–5 December 2019.
88. Wan, Y.; Yang, B.; Xi, X.; Zhang, H.; Ye, Y.; Wang, X. Study on transverse mode instability of fiber lasers with different pump wavelengths. *Infrared Laser Eng.* **2021**, *4*, 196–203.
89. Chu, Q.; Tao, R.; Li, C.; Lin, H.; Wang, Y.; Guo, C.; Wang, J.; Jing, F.; Tang, C. Experimental study of the influence of mode excitation on mode instability in high power fiber amplifier. *Sci. Rep.* **2019**, *9*, 9396. [[CrossRef](#)]
90. Wu, H.; Li, H.; An, Y.; Li, R.; Chen, X.; Xiao, H.; Huang, L.; Yang, H.; Yan, Z.; Leng, J.; et al. Transverse mode instability mitigation in a high-power confined-doped fiber amplifier with good beam quality through seed laser control. *High Power Laser Sci.* **2022**, *10*, e44. [[CrossRef](#)]
91. Zhang, F.; Xu, H.; Xing, Y.; Hou, S.; Chen, Y.; Li, J.; Dai, N.; Li, H.; Wang, Y.; Liao, L. Bending diameter dependence of mode instabilities in multimode fiber amplifier. *Laser Phys. Lett.* **2019**, *16*, 35104. [[CrossRef](#)]
92. Zeng, L.; Wang, X.; Ye, Y.; Wang, L.; Yang, B.; Xi, X.; Wang, P.; Pan, Z.; Zhang, H.; Shi, C.; et al. High Power Ytterbium-Doped Fiber Lasers Employing Longitudinal Vary Core Diameter Active Fibers. *Photonics* **2023**, *10*, 147. [[CrossRef](#)]
93. Ye, Y.; Yang, B.; Shi, C.; Xi, X.; Zhang, H.; Wang, X.; Zhou, P.; Xu, X. Towards power improvement of all-fiber laser oscillators with 30 μm -core Yb-doped fibers by suppressing transverse mode instability. *Laser Phys. Lett.* **2020**, *17*, 85106. [[CrossRef](#)]
94. Wen, Y.; Wang, P.; Yang, B.; Zhang, H.; Xi, X.; Wang, X.; Xu, X. First Demonstration and Comparison of 5 kW Monolithic Fiber Laser Oscillator Pumped by 915 nm and 981 nm LDs. *Photonics* **2022**, *9*, 716. [[CrossRef](#)]
95. Huang, Z.; Shu, Q.; Tao, R.; Chu, Q.; Luo, Y.; Yan, D.; Feng, X.; Liu, Y.; Wu, W.; Zhang, H.; et al. >5 kW Record High Power Narrow Linewidth Laser From Traditional Step-Index Monolithic Fiber Amplifier. *IEEE Photonics Tech. Lett.* **2021**, *33*, 1181–1184. [[CrossRef](#)]
96. Ren, S.; Ma, P.; Li, W.; Wang, G.; Chen, Y.; Song, J.; Liu, W.; Zhou, P. 3.96 kW All-Fiberized Linearly Polarized and Narrow Linewidth Fiber Laser with Near-Diffraction-Limited Beam Quality. *Nanomaterials* **2022**, *12*, 2541. [[CrossRef](#)]
97. Wang, G.; Song, J.; Chen, Y.; Ren, S.; Ma, P.; Liu, W.; Yao, T.; Zhou, P. Six kilowatt record all-fiberized and narrow-linewidth fiber amplifier with near-diffraction-limited beam quality. *High Power Laser Sci.* **2022**, *10*, e22. [[CrossRef](#)]
98. Hong, Z.; Wan, Y.; Xi, X.; Zhang, H.; Wang, X.; Xu, X. High-peak-power pump-modulated quasi-CW fiber laser. *Appl. Opt.* **2022**, *61*, 1826–1833. [[CrossRef](#)]
99. Wang, L.; Zhang, H.; Wang, P.; Yang, B.; Wang, X.; Ning, Y.; Xu, X. Theoretical and Experimental Study of High-Peak-Power High-Brightness Quasi-CW Fiber Laser. *IEEE Photonics J.* **2022**, *14*, 1530206. [[CrossRef](#)]
100. Wang, L.; Zhang, H.; Wang, P.; Yang, B.; Wang, X.; Ning, Y.; Xu, X. A 6.4-kW peak power near-single-mode quasi-continuous wave fiber laser oscillator employing spindle-shaped ytterbium-doped fiber. *Opt. Laser Technol.* **2022**, *154*, 108338. [[CrossRef](#)]

Disclaimer/Publisher's Note: The statements, opinions and data contained in all publications are solely those of the individual author(s) and contributor(s) and not of MDPI and/or the editor(s). MDPI and/or the editor(s) disclaim responsibility for any injury to people or property resulting from any ideas, methods, instructions or products referred to in the content.